(Check for updates)

Two-dimensional covalent organic frameworks with hierarchical porosity

Rong-Ran Liang, (iD) Shu-Yan Jiang, (iD) Ru-Han A (iD) and Xin Zhao (iD) *

Covalent organic frameworks (COFs) are a class of crystalline porous organic polymers assembled by connecting organic building units *via* covalent bonds. They are characterized as extended two-dimensional (2D) or three-dimensional (3D) frameworks with precise spatial structures and building block distribution. A key feature of COFs is their inherent porosity originating from their well-ordered nanopores which are designable, tunable and modifiable through pore engineering. This review describes the pore engineering of 2D COFs based on their framework topologies. It begins with a brief summary of the pore design principles of 2D COFs which are composed of uniform micropores or mesopores. Then the state-of-the-art progress achieved in a new branch of 2D COFs, that is, heteropore COFs, which possess multiple-pore skeletons and thus exhibit hierarchical porosity, is comprehensively reviewed, including their design strategies, synthesis, characterization, properties and applications. In the last part, personal perspectives on this emerging class of 2D polymers with complex structures and hierarchical porosity are discussed.
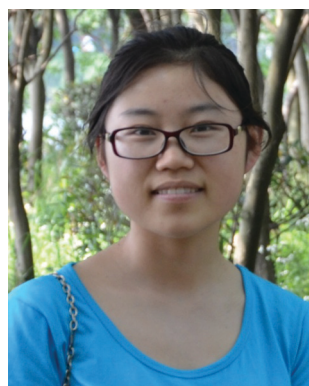
1 Introduction

Over the past century, polymeric materials have played a crucial role in promoting the progress of human civilization by revealing their irreplaceable functions in many aspects of our daily lives. With the increase of the human need for energy and the improvement of the public awareness of environmental

Key Laboratory of Synthetic and Self-Assembly Chemistry for Organic Functional Molecules, Center for Excellence in Molecular Synthesis, Shanghai Institute of Organic Chemistry, University of Chinese Academy of Sciences, Chinese Academy of Sciences, 345 Lingling Road, Shanghai 200032, China. E-mail: xzhao@sioc.ac.cn

protection, the development of new polymeric materials with unique structural features has become an important booster to improve social and technological progress. In this context, porous materials have emerged as the times require and have become one of the focal points in scientific research due to their wide range of applications in gas adsorption, catalysis, optoelectronics, energy storage, *etc.*[1,2] With permanent nanopores inside, porous materials exhibit unique properties and functions compared with non-porous materials. So far, rapid progress has been achieved with the expansion from inorganic porous materials to organic ones. However, most of these porous materials are amorphous and those with well-defined

Rong-Ran Liang was born in Shandong province, China. She received her BS degree in 2014 from the Wuhan University of Technology. In 2019, she completed her PhD in Organic Chemistry under the supervision of Professor Xin Zhao at the Shanghai Institute of Organic Chemistry (SIOC), Chinese Academy of Sciences (CAS). Her current research mainly focuses on the design, synthesis and applications of covalent organic frameworks (COFs).

Rong-Ran Liang

Shu-Yan Jiang was born in 1995. She received her BS degree in 2016 from Nanjing University and is currently pursuing her PhD in organic chemistry under the supervision of Professor Xin Zhao at the Shanghai Institute of Organic Chemistry (SIOC), Chinese Academy of Science (CAS). Her research mainly focuses on the design, synthesis and applications of heteropore covalent organic frameworks.

Shu-Yan Jiang

3920 | *Chem. Soc. Rev.*, 2020, **49**, 3920–3951

This journal is © The Royal Society of Chemistry 2020

internal structures are limited. In this context, covalent organic frameworks (COFs), which have atomically precise structures constructed by covalently linking organic building units into two dimensional (2D) or three dimensional (3D) extended framework structures, have drawn tremendous attention over the past decade.[3–5] Compared with other porous organic polymers (POPs) which are usually amorphous, such as conjugated microporous polymers (CMPs),[6,7] hypercross-linked polymers (HCPs),[8,9] porous aromatic frameworks (PAFs),[10] and polymers of intrinsic microporosity (PIMs),[11,12] the distinct features of COFs are that they have crystalline structures and their structures can be precisely designed, predicted and modified. The porosity and framework structures endow COFs with versatile applications including gas storage,[13–17] separation,[18–22] sensing,[23–28] catalysis,[29–36] proton conduction,[37,38] drug delivery,[39–42] energy storage,[43–50] and optoelectronic devices.[51–56]

To develop COF materials, the pore engineering of COFs, as a fundamental and core subject, is crucial not only for investigating the structure–property relationship, but also for exploring the applications of COFs. In our opinion, the pore engineering of COFs can be divided into two levels. The primary one is to engineer the chemical environment of pores. This level mainly focuses on the chemical constitution of pores, which is dependent on the choice of linkages (covalent bonds formed between the building units upon reticulation) and the nature of skeletons of building units. The linkages, mainly consisting of dynamic covalent bonds (DCBs) such as B–O and C=N bonds, directly affect the crystallization and stability of COFs.[5] On the other hand, the functionalization of COF skeletons through introducing substituent groups, heteroatoms or metal clusters, which can be realized via a premodification or post-functionalization process, is a typical method to tailor the properties of COFs for further applications. This kind of pore engineering, also called channel surface engineering, has been comprehensively summarized in a recent review.[57]

The second level of pore engineering of COFs concentrates on the topological structures of frameworks, which is also the focus of this review. It includes the engineering of the shape, size, and distribution of pores, which can be designed by combining building blocks with various sizes and specific symmetries. Since the pioneering work of Yaghi and co-workers in 2005,[58] plentiful COFs possessing various pore structures have been fabricated. Most of them display homogeneous porosity, possessing only one kind of pores in each framework (here we termed single-pore COFs). So far, the pore types in the polygonal skeletons of single-pore COFs are mainly hexagonal, tetragonal, rhombic and trigonal pores, for which the commonly used design principles are summarized in Fig. 1. They almost follow seven combinations, which are $C_3 + C_2$,[59–63] $C_3 + C_3$,[64–66] $C_4 + C_2$,[67–71] $C_4 + C_4$,[72] $C_2 + C_2$,[73–76] $C_6 + C_2$,[77,78] and T-shaped + C_2.[79] Directed by these combinations, COFs bearing uniform pores with different sizes and shapes could be constructed by the judicious choice of building blocks. Their design strategies and applications have already been comprehensively summarized in some reviews.[80–83]

Although Fig. 1 well demonstrates how uniform pores are periodically distributed in a plane to form 2D networks, this does not mean that COFs can only be produced by tessellations of the same kind of pores. In principle, integrating different kinds of pores into a COF would endow it with a hierarchically porous structure. Natural structures with hierarchical porosity widely exist in biological tissues and are of the essence for the achievement of biological functions. Inspired by such natural structures, many efforts have been made to fabricate artificial materials with hierarchical porosity. Such hierarchically structured materials have been found to possess intriguing properties such as high surface areas, good mass transport, wide distribution of active sites, and minimized diffusion barriers due to the co-existence of hierarchical pores, which facilitate their applications in photocatalysis, supercapacitors, fuel cells, hydrogen storage, solar thermal storage, drug delivery and more.[84–87] Despite the progress achieved, those artificial materials are usually amorphous. To fabricate hierarchically porous materials with highly ordered internal structures is still

Ru-Han A

Ru-Han A received her BE degree in environmental engineering from Shanghai Ocean University in 2014. She is currently pursuing her MS degree in organic chemistry under the supervision of Professor Xin Zhao at the Shanghai Institute of Organic Chemistry (SIOC), Chinese Academy of Sciences (CAS). Her current research focuses on the synthesis and applications of functional heteropore covalent organic frameworks (COFs).

Xin Zhao

Xin Zhao grew up in Yunnan province, China. He received his BS degree in 1994 from Beijing Normal University and PhD degree in 2003 from the Shanghai Institute of Organic Chemistry (SIOC), Chinese Academy of Sciences (CAS). After postdoctoral studies at Harvard University and the University of Chicago, he joined the faculty team of SIOC in May 2008. He is currently a professor at the CAS Key Laboratory of Synthetic and Self-Assembly Chemistry for Organic Functional Molecules. His research interests include porous organic materials, self-assembly, and physical organic chemistry.
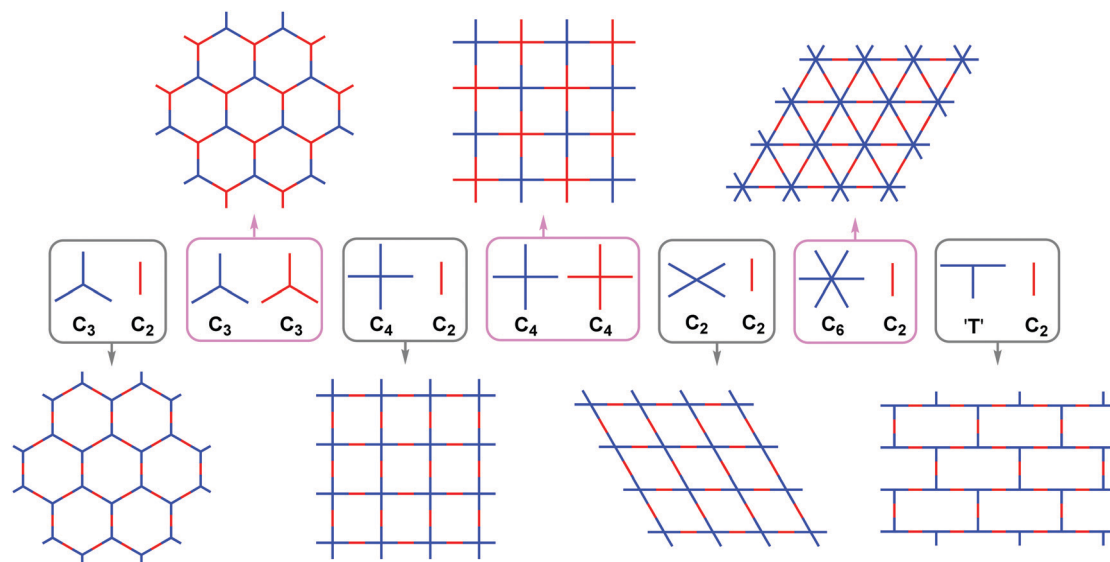
Fig. 1 Topology diagrams showing COFs with various uniform pores obtained through the combination of building blocks with different symmetries.

challenging. In light of their crystalline and designable network structures, COFs should be a superior platform to address this challenge. In 2014, our group initially reported the successful construction of a COF with a periodically ordered distribution of micropores and mesopores (termed the dual-pore COF) (Fig. 2a),[88] following which a series of COFs with hierarchical porosity have been fabricated subsequently (Fig. 2).[89] Compared to those with homogeneous porosity, this new branch of COFs, termed heteropore COFs, possess different types of pores in one framework.[90] In general, it is more difficult to obtain COFs with heterogeneous porosity than those with homogeneous porosity, since the construction of heteropore COFs involves integrating different types of pores into one framework, which undoubtedly increases their structural complexity. In this review, following a brief introduction of general synthesis methods and characterization in the second section, the design strategies that have been already developed for the construction of heteropore COFs and their structural features are systematically introduced in the third section, along with which their properties and applications are further presented. In the fourth section, examples illustrating the advantages and unique applications of heteropore COFs derived from their hierarchically porous structures are demonstrated. In the last part, conclusions and perspectives on heteropore COFs are discussed. It should be noted that a very few COFs were reported to be hierarchical COFs in the literature.[91,92] However, for those COFs, their heterogeneous porosity comes from their hierarchical bulk architectures or different domain structures (for example, core–shell). Therefore, these COFs are not included in this review. Only the crystalline COFs bearing different kinds of well-organized pores in their skeletons, that is, COFs with multiple-pore skeletons, are discussed.
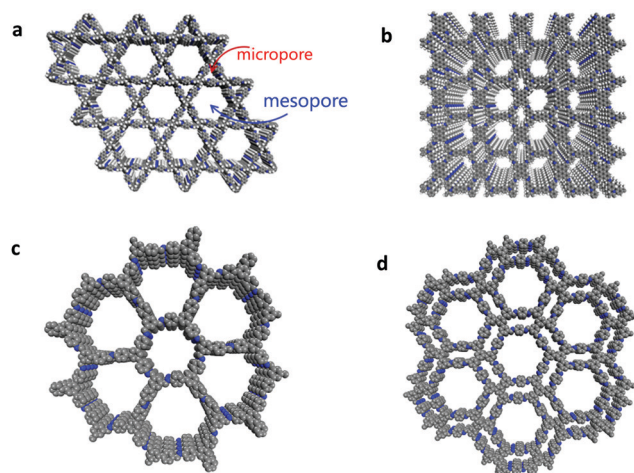
2 General methods for the synthesis and characterization of heteropore COFs

As a new branch of the COF community, the most widely used synthetic method for heteropore COFs is solvothermal condensation. It is the first method used to synthesize COFs and possesses the advantages of promoting the construction of COFs with satisfactory crystallinity and porosity. Generally, solvothermal synthesis is carried out by performing reactions at appropriate temperatures (usually 80–150 °C) for a long period of time (generally several days) in a closed container under an inert atmosphere and by mixing monomers in a suitable solvent system in the presence of a catalyst. Several parameters, such as solvents and temperature, significantly affect the quality of COF products. Thus these parameters need

Fig. 2 Representative framework structures of heteropore COFs. (a) is reproduced from ref. 90 with permission from the Royal Society of Chemistry, copyright 2018. (b) is reproduced from ref. 105 with permission from the Royal Society of Chemistry, copyright 2016.

3922 | *Chem. Soc. Rev.*, 2020, **49**, 3920–3951

This journal is © The Royal Society of Chemistry 2020

to be carefully optimized. Moreover, other factors including the concentration and type of catalyst and reaction time also need to be screened in order to produce COFs with high quality.

The characterization of heteropore COFs is inherited from those of single-pore COFs. Powder X-ray diffraction (PXRD) is the most commonly used technique to determine the crystal structures of heteropore COFs, which are obtained as crystallites from solvothermal reactions. Generally, most crystal structures of heteropore COFs could be elucidated by PXRD analysis in combination with computational simulations. Their lattice parameters are determined by structural refinements, usually Pawley refinement. On the other hand, as they are porous materials, the N_2 sorption measurement is necessary for heteropore COFs, which can not only be used to evaluate their porosity, but also provide pore size distribution (PSD) profiles as supplementary evidence for the determination of their pore structures. In most cases, the heterogeneous pores in a framework can be identified from its PSD profile showing multiple pore size distributions which correspond to the apertures of the different kinds of pores. As to the chemical components and linkages of heteropore COFs, Fourier transform-infrared spectroscopy (FT-IR), ^{13}C cross-polarization magic-angle spinning (CP-MAS) NMR, and elemental analysis can provide detailed information. Their morphologies and particle sizes are characterized through electron microscopy techniques such as scanning electron microscopy (SEM) and transmission electron microscopy (TEM). Furthermore, thermogravimetric analysis (TGA) is used for the evaluation of their thermal stability.

This section briefly introduces the general methods used for the synthesis and characterization of heteropore COFs. While a variety of synthetic methods have been developed for COFs with homogeneous porosity,[80–82] the current preparation method of heteropore COFs mainly relies on solvothermal synthesis. To promote their processing, diversifying their synthesis is highly desired. As for their characterization, with the increase of structural complexity, their structural determination faces more challenges, which is expected to be addressed by the development of advanced techniques. This will be discussed in the last section.

3 Design strategies for 2D heteropore COFs

The complex structures of heteropore COFs make their assembly more difficult, which thus has promoted the development of various design strategies for heteropore COFs. In this section, these strategies are systematically summarized and introduced according to the symmetry of the building blocks and their combinations. Correspondingly, the properties and applications of heteropore COFs are also presented along with specific examples.

3.1   The combination of D_{2h}-symmetric vertexes and linear linkers

D_{2h}-Symmetric monomers are one of the most popular building blocks applied for the fabrication of heteropore COFs, and the
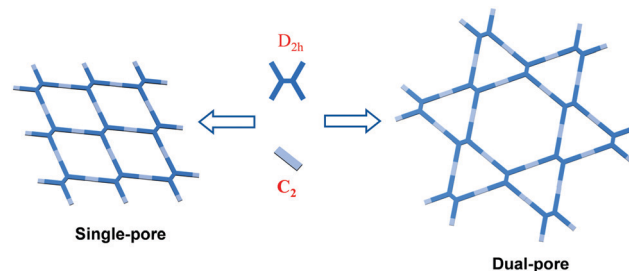

Fig. 3 Cartoon illustration of the generation of COFs with different topological structures formed via the assembly of D_{2h}- and C_2-symmetric building blocks. Adapted from ref. 90 with permission from the Royal Society of Chemistry, copyright 2018.

combination of D_{2h}-symmetric vertexes and linear linkers (C_2-symmetry) is the most frequently used strategy so far. Theoretically, there are two possible frameworks that can be produced from such combinations. One possesses uniform rhombus pores, while the other possesses a Kagome lattice (**kgm** topology) which comprises triangular pores and hexagonal pores (Fig. 3). Due to its dual-pore structure, the latter clearly exhibits hierarchical porosity. In fact, most heteropore COFs reported in the literature possess the Kagome lattice. To investigate this largest member of heteropore COFs reported to date, COFs with **kgm** topology are further categorized according to the different types of linkages as follows.

3.1.1   Connection with the imine linkage. As the most commonly used linkage in the field of COFs, imine bonds possess both good reversibility and stability that satisfy the requirements of facile construction and further applications of COFs. In this context, it is not surprising that most heteropore COFs have also been constructed based on the imine linkage. By taking advantage of imine-linkage chemistry, in 2014, our group realized the construction of the first dual-pore COF (**SIOC-COF**) through the combination of D_{2h}- and C_2-symmetric building blocks,[88] which opened up the door for heteropore COFs. Experimentally, D_{2h}-symmetric tetraphenylethene (TPE)-based tetraamine, 4,4′,4″,4′-(ethene-1,1,2,2-tetrayl)tetraaniline (ETTA), and C_2-symmetric *p*-phthalaldehyde were heated at 120 °C for 4 days in 1,4-dioxane in the presence of aqueous acetic acid (6 M) as a catalyst. The solvothermal condensation reaction afforded yellow crystallites whose crystal structure was elucidated by powder X-ray diffraction and further confirmed by the nitrogen sorption experiment. The experimental PXRD pattern of the dual-pore COF exhibits a large difference from the simulated PXRD patterns of the single-pore structured models. Instead, it well matches the simulated one for the dual-pore structure with staggered (AA) stacking, providing key evidence for the formation of the dual-pore COF (Fig. 4a–f). Furthermore, its nitrogen adsorption and desorption isotherms suggest that the COF possesses both micropores and mesopores, as it displays a combination of type I and type IV isotherms (Fig. 4g). The micropores and mesopores were further identified by PSD analysis, which indicated two main pore distributions at 7.3 and 25.2 Å, respectively, with the former corresponding to the pore size of the triangular pores while the latter matching the

This journal is © The Royal Society of Chemistry 2020

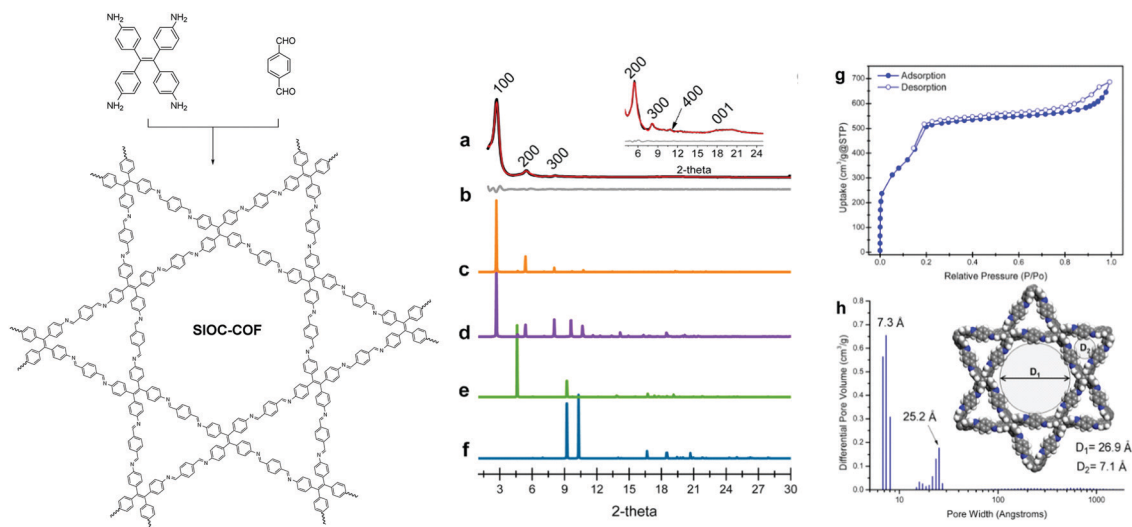*Chem. Soc. Rev.*, 2020, **49**, 3920–3951 | **3923**

Fig. 4 Left: synthesis and structure of the **SIOC-COF**. Right: (a) experimental (black) and refined (red) PXRD patterns of the **SIOC-COF**; (b) difference plot between the experimental and refined PXRD patterns, and simulated PXRD patterns of (c) dual-pore-AA structure, (d) dual-pore-AB structure, (e) single-pore-AA structure, (f) single-pore-AB structure; (g) N_2 adsorption and desorption isotherm curves and (h) pore size distribution profile of the **SIOC-COF**.[88] Reproduced from ref. 88 with permission from American Chemical Society, copyright 2014.

aperture of the hexagonal pores quite well (Fig. 4h). Molecular mechanistic calculations indicate that the dual-pore models have much lower total energies compared with their single-pore isomers and the dual-pore structure with AA stacking is the most thermodynamically favorable product. This COF exhibits good chemical and thermal stabilities. Its potential as a hydrogen storage material was further investigated and it was found to display a H_2 uptake of 1.37 wt% at 77 K and 1 bar.

In 2016 this dual-pore COF was also reported by Bein and co-workers to demonstrate a synthetic concept to reduce the stacking faults and dislocations of COF layers.[93] ETTA has a propeller-shaped conformation and plays a role as a docking site during the process of attachment of successive building blocks. As a result, consecutive COF sheets can be locked in a specific position during crystal growth (Fig. 5), which results in a high degree of crystallinity of the COF.

On the other hand, due to its structural peculiarity arising from bearing both micropores and mesopores, the **SIOC-COF** was further used as a typical example of dual-pore COFs by Jiang et al. to investigate iodine capture in 2018. The COF showed a high iodine uptake capacity of up to 4.79 g g^{-1}, corresponding to 100% pore occupation.[94] This result suggests that different types of pores in the dual-pore COF do not interfere with each other in the process of iodine uptake. In 2019, Ke et al. developed a method to integrate this dual-pore COF into a 3D printing material.[95] In their design, a 3D-printable homogeneous hydrogel consisting of imine polymer/Pluronic F127 was firstly prepared through intentionally restraining the degree of polymerization of the amorphous polyimine by introducing a large excess of water and controlling the amount of acid catalyst and aniline to form an imine intermediate. Then an amorphous-to-crystalline transformation was achieved after 3D printing. Upon the removal of F127, a 3D monolith with high crystallinity and high surface area was obtained.
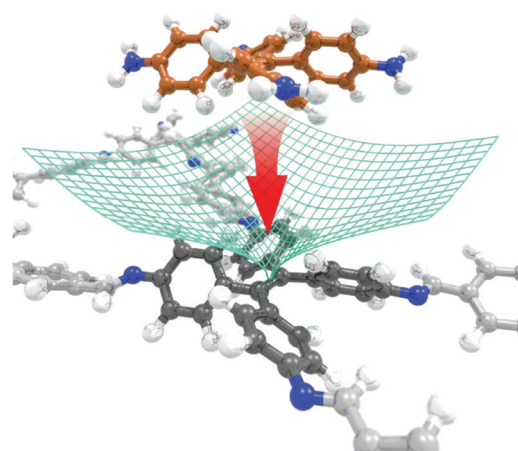

Fig. 5 Illustration of the guided attachment of the TPE-based building blocks (C, dark grey for the four core aromatic rings, light grey for the other carbons; N, blue; H, white). The molecular conformation of this building block (dark grey) causes a single minimum in the potential-energy hypersurface (green grid) for lateral displacement, which allows the successive layer (C, orange; N, blue; H, white) to lock in position (shown by a red arrow).[93] Adapted from ref. 93 with permission from Springer Nature, copyright 2016.

The successful fabrication of COF monoliths provides opportunities for the future applications of COFs with sophisticated 3D architectures.

Encouraged by the successful synthesis of the dual-pore COF, obtaining COFs with a higher level of hierarchical porosity was further pursued. In 2016, we achieved this goal through a heterostructural mixed linker strategy.[96] The implementation of this strategy involves a three-component assembly of a D_{2h}-symmetric building block and two C_2-symmetric linkers with different lengths. In detail, when ETTA was condensed with a dialdehyde longer than terephthalaldehyde (TPA), for
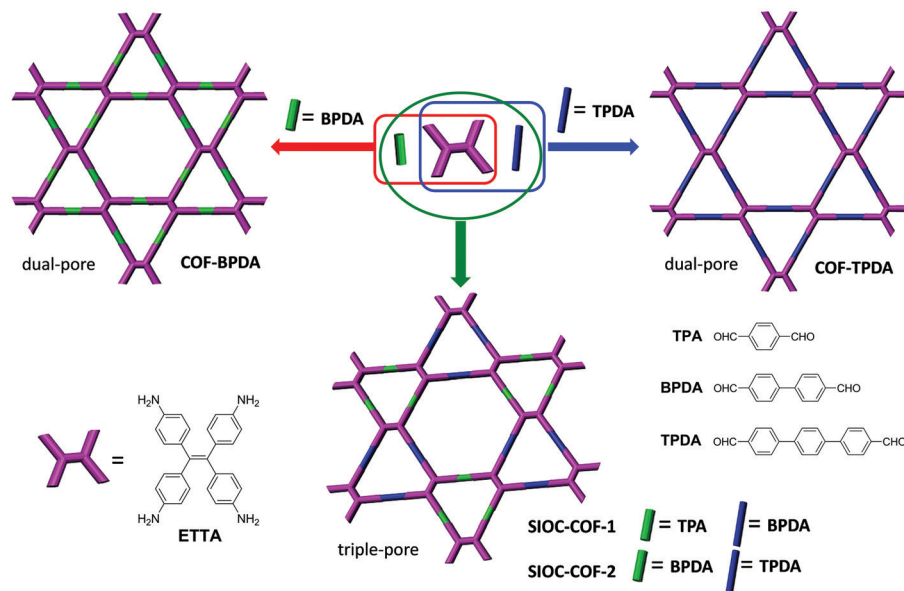
3924 | *Chem. Soc. Rev.*, 2020, **49**, 3920–3951

This journal is © The Royal Society of Chemistry 2020

Fig. 6 Cartoon representation of the synthesis of dual-pore and triple-pore COFs.[96] Adapted from ref. 96 with permission from American Chemical Society, copyright 2016.

example, [1,1′-biphenyl]-4,4′-dicarbaldehyde (BPDA) or [1,1′:4′,1″-terphenyl]-4,4″-dicarbaldehyde (TPDA), dual-pore COFs similar to the **SIOC-COF** but with larger pore sizes (**COF-BPDA** and **COF-TPDA**) were produced (Fig. 6, top). By contrast, the condensation of ETTA, TPA and BPDA or ETTA, BPDA and TPDA in a 1 : 1 : 1 ratio afforded COFs bearing three different types of pores (triple-pore COFs, **SIOC-COF-1** and **SIOC-COF-2**) (Fig. 6, bottom). Similar to the system based on the two-component assembly of ETTA and dialdehyde, theoretically the three-component assembly also would result in triple-pore and single-pore COFs. The obtention of the triple-pore COFs by polymerization, instead of the single-pore ones, was confirmed by the PXRD data and PSD analysis. Particularly, the PSD analysis clearly exhibits three pore size distributions for the as-prepared COFs, with 7.3, 11.8 and 30.6 Å for **SIOC-COF-1** and 11.3, 13.8 and 32.7 Å for **SIOC-COF-2**, which correspond to small triangular micropores, large triangular micropores, and hexagonal mesopores, respectively. The successful construction of the triple-pore COFs suggests the great potential of this mixed linker strategy for the fabrication of COFs with higher hierarchy and complexity. It is anticipated that more complex structures may be obtained by introducing more kinds of building blocks in one condensation reaction.

Driven by their distinctive structures, more heteropore COFs with **kgm** topology have been reported successively by using different types of linear monomers for different applications. In 2018, Fang *et al.* reported a dual-pore COF (**ETTA-TFA-COF**) containing fluorine atoms through the condensation of ETTA and 2,3,5,6-tetrafluoro-benzene-1,4-dicarbaldehyde (Fig. 7).[97] Thanks to the hydrophobicity of fluorine atoms, the **ETTA-TFA-COF** exhibits excellent stability in alkaline solutions. In the same year, taking ETTA and dialdehyde benzo[1,2-*b*:4,5-*b*′]-dithiophene-2,6-dicarboxaldehyde (BDT) as monomers, Bein and co-workers fabricated a photoactive porous framework with

Kagome lattices (**BDT-ETTA COF**) (Fig. 7).[98] To evaluate its photochemical activity as an electrode, the **BDT-ETTA COF** was grown on transparent conductive fluorine doped tin oxide (FTO) and indium tin oxide (ITO) substrates to form films. Due to its structural features and the use of a donor-type dithiophene, the dual-pore COF films exhibit remarkable water stability, efficient light harvesting properties and suitable band positions, thus becoming viable photocathodes for light-driven water reduction. Lately, by taking advantage of the electrophoretic deposition (EPD) technique for depositing COFs to afford COF films, they further improved the photoelectrochemical catalytic performance of EPD **BDT-ETTA COF** films for photocatalytic water reduction.[99] Moreover, taking the **BDT-ETTA COF** and another similar dual-pore COF (**4PE-TT COF**, Fig. 7) as two of three examples, Bein *et al.* investigated the electronic processes and optical properties of a series of conjugated 2D COFs using highly sensitive optical spectroscopy techniques, thus presenting a unified model in which charges are produced through rapid singlet–singlet annihilation and exhibiting lifetimes as long as several tens of microseconds.[100] In 2019, by replacing *p*-phthalaldehyde with 2,3-dihydroxy-benzene-1,4-dicarbaldehyde (2,3-Dha), we synthesized a homologous COF of **SIOC-COF** (**COF-ETTA-2,3-Dha**, Fig. 7).[101] Benefiting from the intramolecular hydrogen-bonding interactions originating from the introduction of the catechol segment, **COF-ETTA-2,3-Dha** exhibits extremely high stability against water under different pH conditions. Its chemical stability and its hierarchical porosity make this dual-pore COF an excellent material for the removal of Cd(II) from aqueous solutions with a very rapid adsorption rate, high adsorption capacity, and good recyclability.

With the aim of expanding the types of reactions for facile post-synthetic functionalization, in 2020, Yaghi and co-workers developed a new dual-pore Kagome COF (**COF-616**) bearing
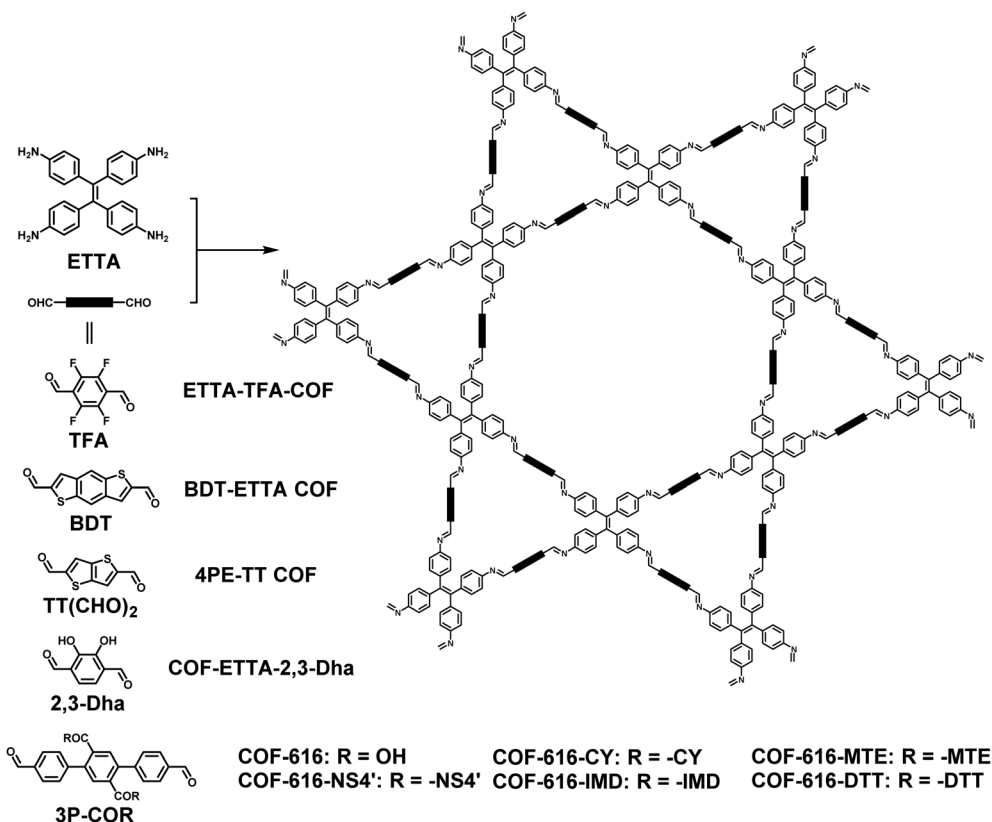
Fig. 7 Synthesis of **ETTA-TFA-COF**, **BDT-ETTA COF**, **4PE-TT COF**, **COF-ETTA-2,3-Dha** and **COF-616** series.[97,98,100–102]

carboxyl groups with ETTA and *p*-terphenyl-2′,5′-dicarboxylic acid-4,4″-dicarboxaldehyde (3P-COOH) as monomers (Fig. 7).[102] The pre-installed carboxyl groups of **COF-616** were then found to be amenable to post-synthetic amidation, esterification, and thioesterification reactions, which provides a facile method to introduce various complex payloads on COFs. As a proof of concept, various chelating functional groups, including *N,N*-bis(2-((2-(ethylthio)ethyl)thio)ethyl)amine (NS4′), cyclam (CY), 1-(1*H*-imidazol-2-yl)-*N*-methylmethanamine (IMD), 2-(methythio)ethanol (MTE) and dithiothreitol (DTT), were successfully incorporated into **COF-616**, yielding a family of adsorbents which exhibit excellent performance for the removal of various contaminants from water.

In addition to ETTA described above, several other TPE-based D_{2h}-symmetric building blocks have also been designed and applied for the construction of 2D dual-pore COFs with Kagome lattices, which improves the chemical diversity of this fascinating topological structure. In 2018, Zhao and co-workers exploited a building block containing an aggregation-induced emission (AIE) rotor-active tetraphenylethylene (TPE) moiety, 1,1,2,2-tetrakis(4-formyl-(1,1′-biphenyl))-ethane (TFBE), to fabricate dual-pore COFs with **kgm** topology (**NUS-30** and **NUS-32**) by its condensation with hydrazine or 1,4-diaminobenzene (Fig. 8a).[103] Following the mixed linker strategy,[96] a triple-pore COF (**NUS-31**) was also synthesized by three-component condensation of TFBE, hydrazine and 1,4-diaminobenzene. These isostructural bulk COFs were further exfoliated into ultrathin 2D nanosheets with a thickness
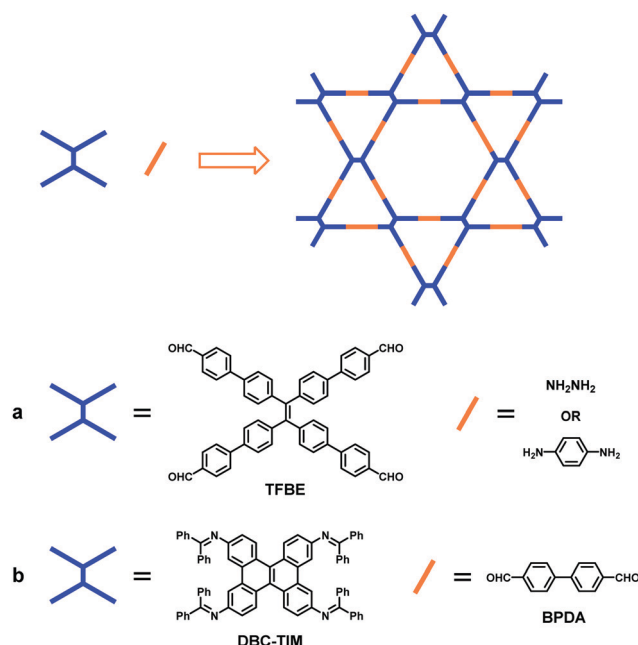

Fig. 8 Construction of **kgm** topology COFs with various monomers.[103,104]

of around 2–4 nm by a temperature-swing gas exfoliation approach. The conformational restriction of TPE molecular rotors through covalent bonds in the confined 2D frameworks

3926 | *Chem. Soc. Rev.*, 2020, **49**, 3920–3951

This journal is © The Royal Society of Chemistry 2020

leads to suppressed AIE characteristics of the nanosheets, inducing the signal amplification effect upon recognition of biomolecules such as amino acids and pharmaceutical molecules (L-dopa). In 2019, Chen *et al.* designed a new D_{2h}-symmetric dibenzo[*g,p*]chrysene (DBC)-based building block (DBC-TIM) (Fig. 8b).[104] The DBC unit could be recognized as the "closed" form of the TPE unit with a large conjugated structure, in which two additional C–C single bonds are introduced to connect the phenyl rings. As a result, the condensation of DBC-TIM and 4,4′-biphenyldicarbaldehyde (BPDA) led to the formation of a highly crystalline dual-pore COF (**DBC-2P**) with strong interlayer interactions, which contribute to the excellent stability of the COF in strong acids, bases and boiling water. Taking advantage of its excellent chemical stability and ordered nanochannels, **DBC-2P** was further applied for the encapsulation of linear polyethylene glycol (PEG) and PEG-LiBF$_4$ salts in its nanochannels, which generated hybrid materials for the investigation of ionic conductivity. The hybrid material displays a high ionic conductivity of 2.31×10^{-3} S cm^{-1}, suggesting the great potential of the hybridization of COFs and polymers as a broad platform for further improving their physical and chemical properties.

Apart from the TPE-based D_{2h}-symmetric building blocks described above, other monomers with D_{2h} symmetry have also been exploited. In 2016, our group reported another two monomers with D_{2h} symmetry, [1,1′-biphenyl]-3,3′,5,5′-tetracarbaldehyde (BTA) and 4,4′,4″,4‴-([1,1′-biphenyl]-4,4′-diylbis(azanetriyl))tetrabenzaldehyde (BDTB).[105] To diversify COF structures with Kagome lattices, BTA was used for the construction of two dual-pore COFs (**COF-BTA-DAB** and **COF-BTA-BZ**, Fig. 9) with 1,4-diaminobenzene (DAB) and benzidine (BZ) being used as linear linkers.[106] In 2019, using BTA as one of the monomers, we further synthesized a new dual-pore Kagome COF (**COF-BTA-DHBZ**, Fig. 9) in which hydroxyl groups were introduced as functional sites for the adsorptive removal of Cr(VI) from aqueous solutions.[107]
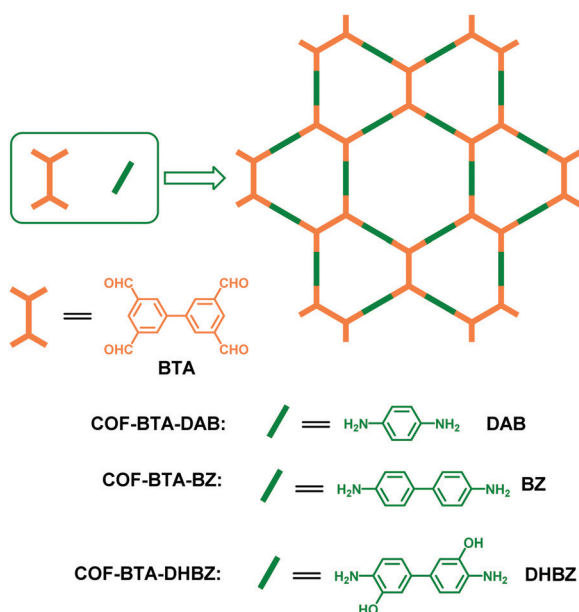
This dual-pore COF shows a fast removal rate (272 Cr mg g^{-1} within 10 min) and a high adsorption capacity of 384 mg g^{-1} Cr, which is among the highest uptake of Cr(VI) by porous materials reported so far. The mechanistic study reveals that the introduction of hydroxyl groups on the COF skeleton is the key point for the efficient removal of Cr(VI).

In 2019, Auras *et al.* reported three new dual-pore COFs with **kgm** topology (**Per-1P COF**, **Per-N COF** and **Per-Py COF**) synthesized through the combination of 2,5,8,11-tetrakis(4-aminophenyl)perylene (Per(NH$_2$)$_4$) and linear monomers (Fig. 10a).[108] They investigated the acid vapor sensing of these COFs by taking advantage of the basicity of imine bonds, using which the function of linkages was exploited.[109,110] They found that the imine bonds in the COFs exhibited reversible protonation *via* a two-step process, from which mono- and bisprotonated species could be generated, respectively (Fig. 10b). The two protonated species have distinct absorption features in the red and near-infrared spectral regions. Therefore, these COFs could act as colorimetric sensors, which are capable of determining the acid strength and concentration simultaneously in nonaqueous solutions. Furthermore, the COF films, grown on fused silica, sapphire, or indium tin oxide coated glass substrates, could detect acid vapor to a very low limit and possess a response range of at least 4 orders of magnitude.

Since the combination of D_{2h}- and C_2-symmetric building blocks would potentially result in both single-pore and dual-pore framework structures as mentioned above (Fig. 3), it is also of interest to selectively synthesize the two structures because they are constitutional isomers. Single-pore COFs prepared from such a combination have also been realized when a monomer other than ETTA was used.[111,112] The construction of both single-pore and dual-pore COFs from the same D_{2h}-symmetric monomers is challenging and rarely reported. The earliest report on the selective synthesis of both frameworks could be dated back to 2017, when we realized the individual construction of single-pore and dual-pore COFs by the condensation of ETTA and different dialdehydes.[113] Our idea is to introduce substituents into the skeleton of terephthalaldehyde. Since the internal diameter of the triangular micropores of the **SIOC-COF** is just around 0.7 nm, it can only accommodate substituents of small size. Substituents with larger sizes would result in significant steric repulsion and thus prevent the formation of triangular pores. Alternatively, a single-pore framework might be generated because of its larger rhombic pores. To validate our design, we chose three TPA derivatives with different substituents at 2,5 positions, that is, 2,5-dihydroxyterephthalaldehyde (DHTA), 2,5-diethoxyterephthalaldehyde (DETA) and 2,5-dibutoxyterephthalaldehyde (DBTA). By using the same [D_{2h} + C_2] combination, the condensation of ETTA with these TPA derivatives would give rise to COFs with different topological structures depending on the size of the substituents. This design strategy did work. By the combination of ETTA and DHTA, a dual-pore COF was generated. In contrast, the condensation of ETTA with DETA or DBTA afforded single-pore frameworks (Fig. 11). These results demonstrate that the steric effect of substituents could play a crucial role in the regulation of the topological structures of 2D COFs. However, it
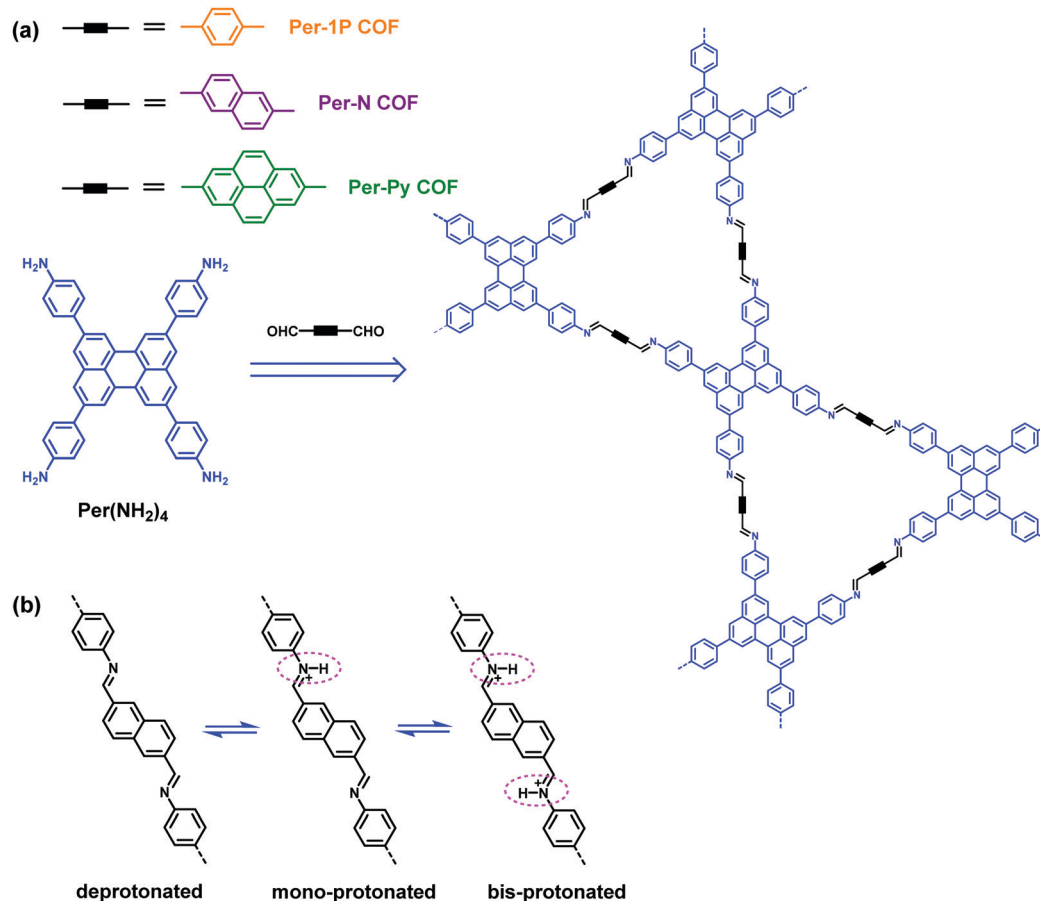

Fig. 9 Construction of BTA-based COFs.[106,107]

This journal is © The Royal Society of Chemistry 2020

Chem. Soc. Rev., 2020, **49**, 3920–3951 | **3927**

Fig. 10 (a) Synthesis of the **Per-1P COF**, **Per-N COF** and **Per-Py COF**. (b) The stepwise protonation of imine-linked bridges of the **Per-N COF**.[108] Adapted from ref. 108 with permission from American Chemical Society, copyright 2019.
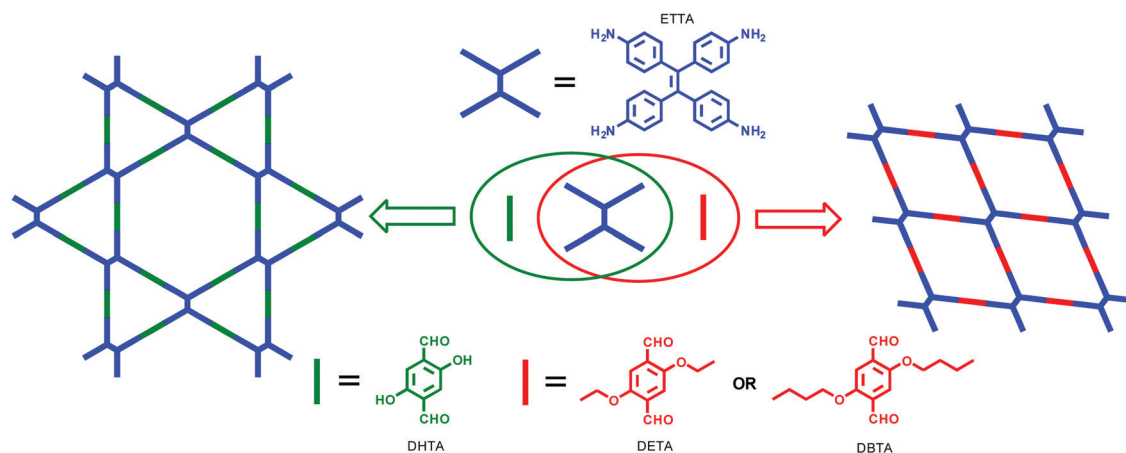

Fig. 11 Synthesis of the dual-pore COF and single-pore COFs from ETTA and dialdehydes with different substituents, demonstrating the significant influence of substituents on the topologies of COFs.[113]

should be noted that the dual-pore COFs and single-pore COFs obtained in this work are not constitutional isomers because they have different chemical compositions.

While mixtures of single-layered COF isomers assembled through the condensation of D_{2h}- and C_2-symmetric building blocks on a graphite surface were observed by Wang and

co-workers by scanning tunneling microscopy (STM),[114] it is not until very recently that the bulk synthesis of constitutional isomers of a COF has been realized.[115] In 2020, we found that the single-pore and dual-pore COFs could be obtained in a controllable and selective way by changing the solvent systems used for the solvothermal condensation of D_{2h}-symmetric
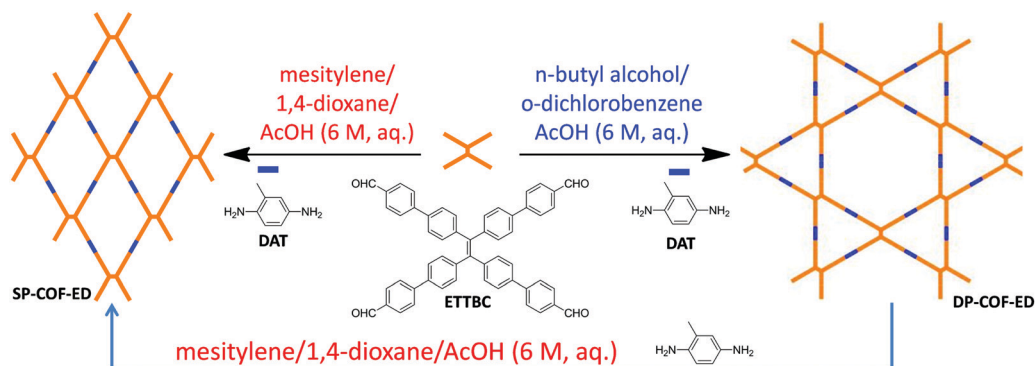
Fig. 12 Controllable synthesis of **SP-COF-ED** and **DP-COF-ED** isomers and the transformation from one isomer to the other.[115] Reproduced from ref. 115 with permission from Chinese Chemical Society, copyright 2020.

4′,4′′′,4′′′′′,4′′′′′′′-(ethene-1,1, 2,2-tetrayl)tetrakis([1,1-biphenyl]-4-carbaldehyde) (ETTBC) and C_2-symmetric 2,5-diaminotoluene (DAT) (Fig. 12).[115] As expected for isomers, the two COFs display different properties, as indicated by the distinct differences in their gas/vapor adsorption behavior and chemical stability. Moreover, structural transformation from the dual-pore COF isomer to the single-pore COF isomer has been realized.

3.1.2 Connection with the boronate linkage. Apart from those constructed based on imine linkages, a Kagome COF fabricated using a boronate linkage has also been reported. In 2016, Jiang's group reported a TPE-cored boronic acid (TPEBA) which could be deemed as a structure generated by replacing the four amino groups on ETTA with boronic acids.[116] The condensation of TPEBA and 1,2,4,5-tetrahydroxybenzene (THB) afforded a dual-pore COF with the Kagome lattice (**TPE-Ph COF**, Fig. 13). This dual-pore COF was found to be highly

luminescent with an exceptionally high quantum yield. This was attributed to the synergistic effect of intralayer covalent bonding and interlayer π–π stacking interactions, which prevented the distortion of the excited state and thus enabled the excited energy release *via* fluorescence decay. Taking advantage of the high emission feature, the **TPE-Ph COF** was further explored as a fluorescence sensor for ammonia. It exhibited very high sensitivity towards gaseous ammonia, with the detection limit down to the sub ppm level.

3.1.3 Connection with the amide linkage. A nice method to prepare heteropore COFs with other linkages is the linkage transformation reported by Yaghi and co-workers in 2016. They selected the **SIOC-COF** (named **4PE-1P-COF** in their paper) as an example to demonstrate how to transform the imine linkage into the amide linkage in COFs by oxidation (Fig. 14).[117] Through reaction optimization, a mild oxidative condition was established using sodium chlorite, acetic acid, and
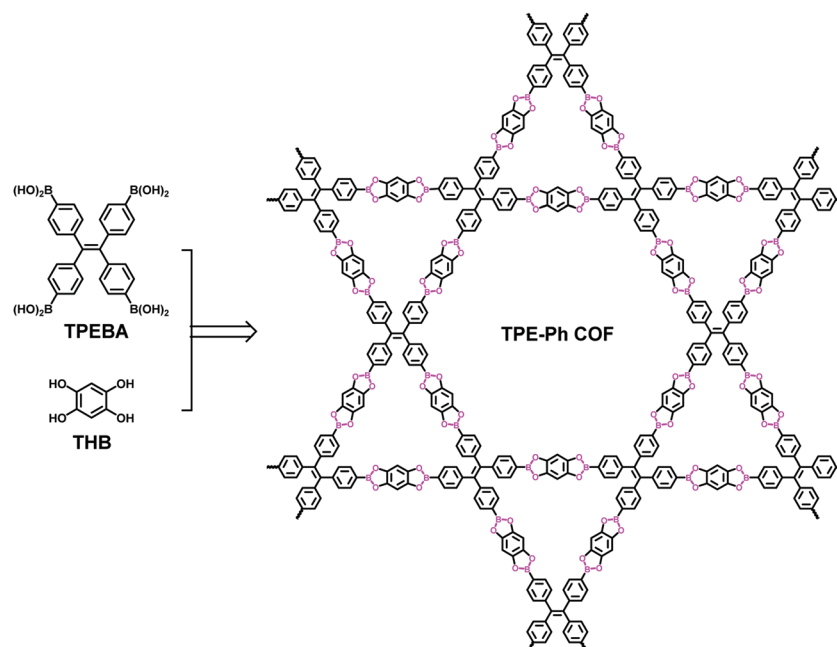

Fig. 13 Synthesis of the **TPE-Ph COF**.[116]

This journal is © The Royal Society of Chemistry 2020

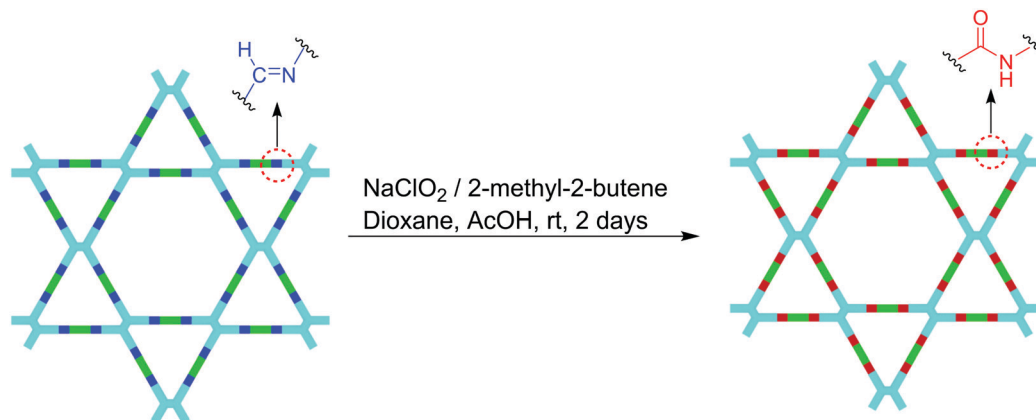*Chem. Soc. Rev.*, 2020, **49**, 3920–3951 | **3929**

Fig. 14 An amide-linked Kagome dual-pore COF constructed by the oxidation of the linkages of its corresponding imine-linked framework.[117]

2-methyl-2-butene in 1,4-dioxane, by which the crystallinity and permanent porosity of the pristine COF were retained. The resulting amide-linked COF shows enhanced chemical stability under aqueous acidic and alkaline conditions compared with its pristine COF with the imine linkage. This method provides a feasible way to fabricate COFs which are difficult to obtain or even inaccessible by the direct condensation of monomers. An advantage of this method is that the crystallization problem usually encountered in direct COF synthesis can be bypassed.

3.1.4 Connection with carbamate and thiocarbamate linkages. In 2019, Yaghi and co-workers further extended the linkage transformation approach from one-pot reaction to

multistep synthesis. Starting from a new **kgm** lattice COF (**COF-170, 1**), which was synthesized through the condensation of (E)-3,3′,5,5′-tetrakis-(4-aminophenyl)stilbene (TAPS) and 3,5-dimethoxyterephthalaldehyde (DMTP) under solvothermal conditions, they successfully realized the synthesis of isostructural cyclic carbamate- and thiocarbamate-linked COFs (**4** and **5**) through three consecutive postsynthetic modifications, which are demethylation of the methoxy groups in COF **1** to afford COF **2**, reduction of the imine linkage to generate **3**, and reaction with 1,1′-carbonyldiimidazole (CDI) or 1,1′-thiocarbonyldiimidazole (TCDI) to finally give rise to COF **4** or COF **5** (Fig. 15).[118] Among these polymers, amine-linked **3** was found to be noncrystalline
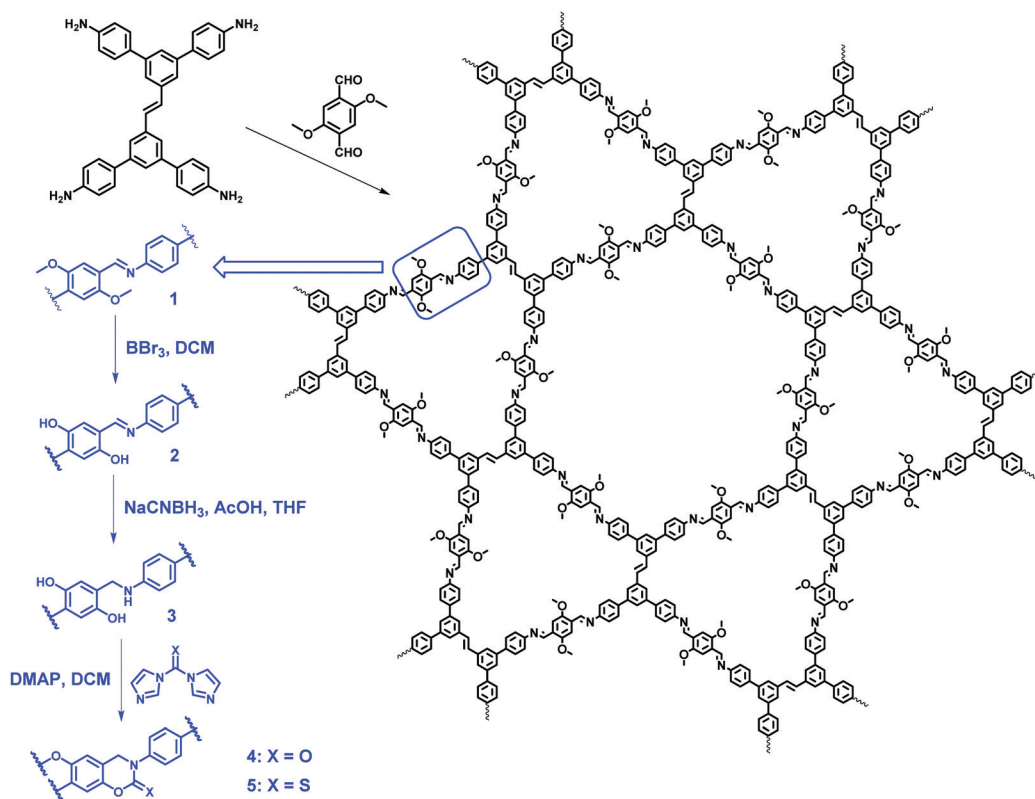

Fig. 15 Transformation of the imine linkage to construct cyclic carbamate- and thiocarbamate-linked dual-pore COFs.[118]

and less porous, while the other polymers are crystalline and porous, indicating significant conformational and structural changes at each step and the important roles the noncovalent interactions and conformational flexibility played in COF crystallinity and porosity. Moreover, they realized the first quantitation of yields in the reactions for COF postsynthetic modification by using ^{15}N multiCP-MAS NMR spectroscopy. This work extends the precision of organic solution-phase synthesis to extended frameworks, representing a significant step not only in the field of COFs, but also in synthetic chemistry.

3.1.5 Aminal-linked heteropore COFs. In 2019, we reported two unique dual-pore COFs linked by aminal units through D_{2h}-symmetric tetraaldehydes and secondary amines as monomers.[119] The formation of aminal is similar to that of the imine bond, which can be regarded as the product of an imide bond being attacked by another amine. This reaction has good reversibility but it requires a conformational transformation from the planar sp^2-hybridization of carbonyl carbon to the tetrahedral sp^3-hybridization of aminal carbon. In this work, two aminal-linked 2D COFs (**Aminal-COF-1** and **Aminal-COF-2**) were constructed through the condensation of piperazine with D_{2h}-symmetric tetraaldehydes (A1 and A2) (Fig. 16). The successful construction of the aminal-linked COFs is attributed to two factors. Firstly, the nonplanar feature of these tetraaldehydes can accommodate the space change in the sp^2-to-sp^3 transformation process. Secondly, the use of piperazine, a secondary amine, can impede the formation of imine bonds. The aminal linkages are confirmed by FT-IR spectra, ^{13}C and ^{15}N CP/MAS NMR, XPS spectra and hydrolysis experiments.

The as-obtained COFs have good crystallinity and crystallize in the **cpi** net. This is a new topology previously not reported for COFs. Moreover, this work adds a new member to the linkage chemistry of COFs. Unlike other 2D COFs with unsaturated or planar linkages, the tetrahedral geometry and nonconjugated feature of the aminal linkage enable the properties of monomers to be maintained to a large extent. The solid-state fluorescence spectra revealed that the aminal-COFs possess almost the same emission wavelengths as that of their monomers. Therefore, this type of linkage is expected to achieve more accurate prediction and regulation of the properties of COFs, which is helpful for the custom synthesis of functional COFs.

3.2 The combination of two D_{2h}-symmetric building blocks

In 2016, we developed a $[D_{2h} + D_{2h}]$ strategy to construct dual-pore COFs through assembling two D_{2h}-symmetric building blocks. As shown in Fig. 17, ETTA is condensed with BTA or BDTB to give rise to two dual-pore COFs both bearing two kinds of micropores (**SIOC-COF-5** and **SIOC-COF-6**).[105] Benefiting from their microporous characteristics, these two dual-pore COFs show good capture capacities for CO_2 and H_2, with the CO_2 uptake of **SIOC-COF-5** reaching 19.8 wt% (273 K, 1 bar) and the H_2 uptake of **SIOC-COF-6** reaching up to 1.79 wt% (77 K, 1 bar).

3.3 The combination of D_{2h}-symmetric and C_4-symmetric building blocks

In 2019, Lan *et al.* reported a $[D_{2h} + C_4]$ strategy to fabricate a series of dual-pore COFs (**TTCOF-M**) through assembling
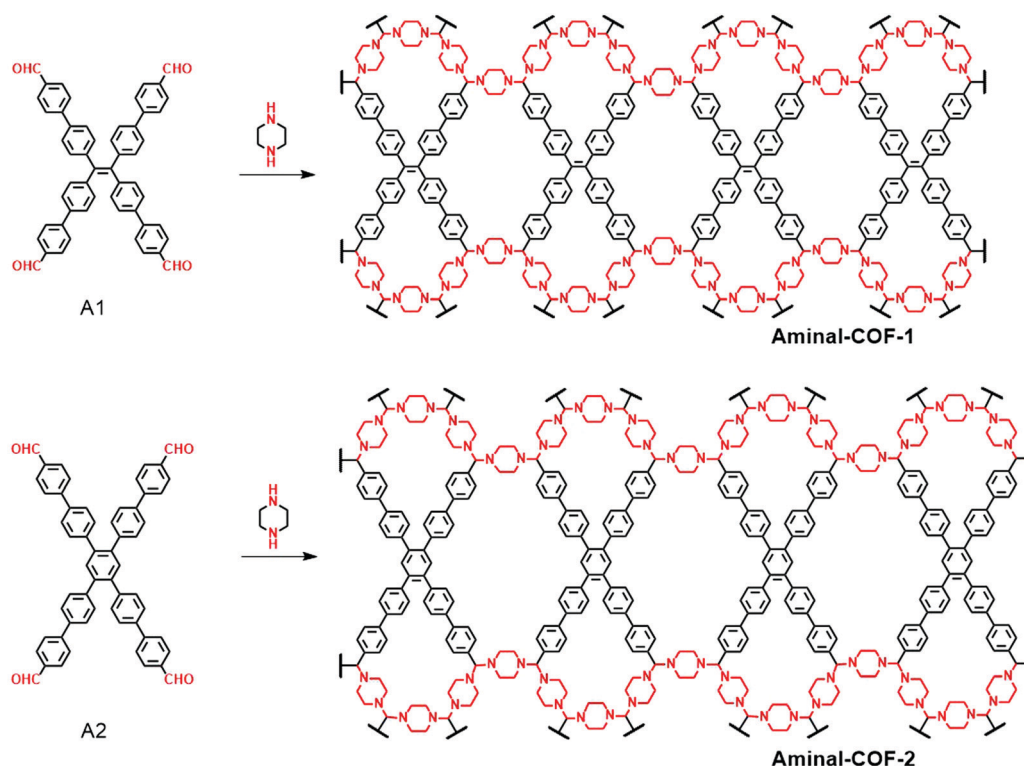

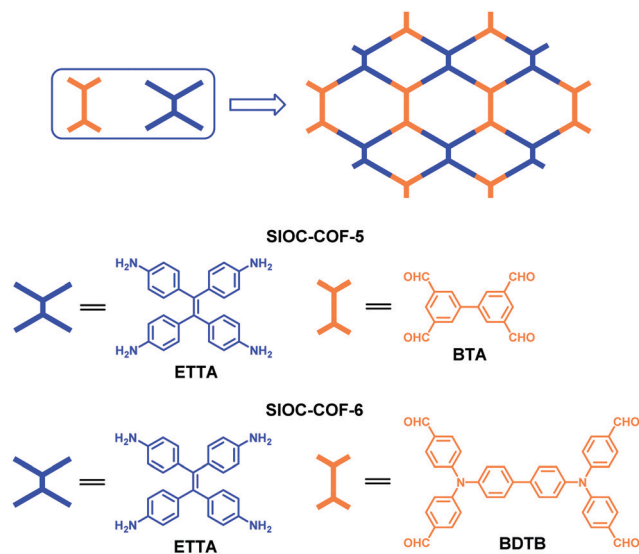**Fig. 16** Synthesis of **Aminal-COF-1** and **Aminal-COF-2**.[119]

Fig. 17 Construction of **SIOC-COF-5** and **SIOC-COF-6**.[105]

D_{2h}-symmetric 2,3,6,7-tetra(4-formylphenyl)-tetrathiafulvalene (TTF) with C_4-symmetric metallized 5,10,15,20-tetrakis(4-amino-phenyl)-porphinato (TAPP-M, M = 2H, Zn, Ni, Cu) (Fig. 18).[120] In their design, the integration of TTF and TAPP could enable the the efficient separation and transfer of photoexcited electrons in the framework, due to the electron-deficient feature and good visible-light collecting ability of metalloporphyrin and the rapid electron transfer of the electron-rich tetrathiafulvalene structure. As expected, **TTCOF-Zn/Cu** COFs were revealed to possess suitable photocatalytic redox potentials. These COFs were then used as photocatalysts for reducing CO_2 with H_2O as an electron donor, which exhibited high photocatalytic activity and selectivity with **TTCOF-Zn** showing the highest CO production (12.33 mmol) and selectivity (ca. 100%). It should be noted that, although the combination of the angles of the building blocks seems to be not ideal for the construction of the COFs, the target products with

high crystallinity and good yields (81% for **TTCOF-Zn**) could still be obtained. This might be attributed to tension release through twisting imine bonds and/or the framework structures.

3.4 The combination of D_{2h}-symmetric and C_3-symmetric building blocks and the strategy of sub-stoichiometry

Generally, the formation of fully condensed network structures is taken as a prerequisite for the design of COFs. However, the sub-stoichiometry of building blocks might provide more possibilities for the construction of COFs with interesting topological structures. A sub-stoichiometric method to fabricate heteropore COFs was reported by Lotsch et al. in 2019.[121] They selected D_{2h}-symmetric tetragonal pyrene tetraaniline (P) and C_3-symmetric trigonal triazine tribenzaldehyde (T) or benzene tripicolinaldehyde (Y) as monomers. Theoretically, 2D COFs could not be obtained through the combination of [4+3] if all functional groups participate in the condensation reaction. Interestingly, two sub-stoichiometric 2D COFs (**PT-COF** and **PY-COF**) were successfully constructed with the feed ratio of P and T or Y being 1 : 1. These two COFs feature **bex** net topology and periodic uncondensed amine functionalities (Fig. 19). The remaining amine groups could enhance CO_2 adsorption, act as organocatalysts or be derivatized in a subsequent reaction. Moreover, COFs with **bex** topological structures can also be realized through the combination of [4+3+2]. In this work, the **PT₂B-COF** and **PY₂B-COF** were further fabricated through the condensation of P, T/Y and linear ditopic benzidine (B) (Fig. 19), indicating the necessity of increasing additional components and adjusting the reaction ratios for the construction of COFs with a higher degree of complexity and hierarchy.

In the same year, Yaghi and co-workers also reported another sub-stoichiometric 2D COF with the same combination of D_{2h}- and C_3-symmetric building blocks as mentioned above, but with different feed ratios.[122] At a feed ratio of 3/2, a COF with defective **tth** topology (**COF-340**) was obtained through the condensation of 1,3,5-tris(p-formylphenyl)benzene (TFPB) and
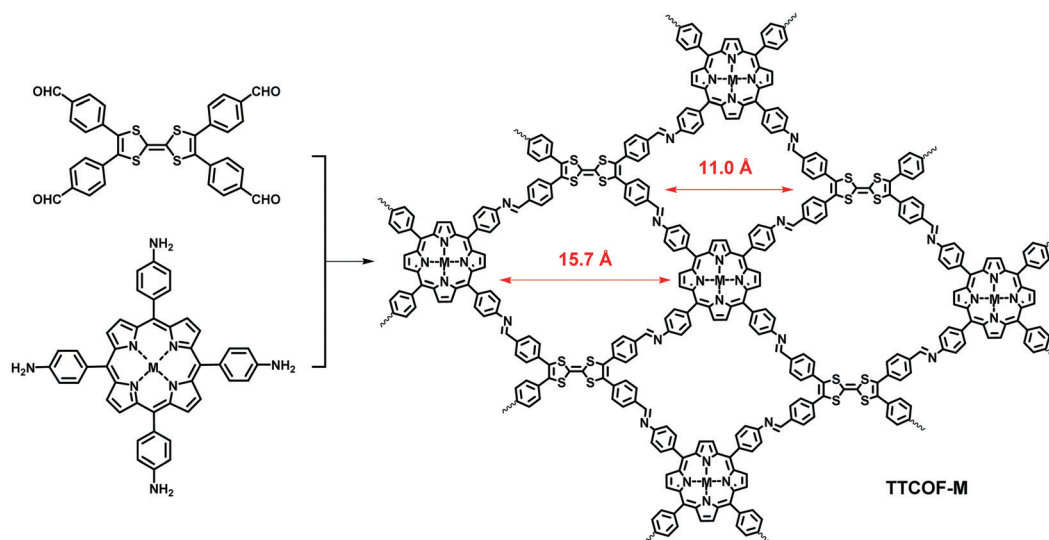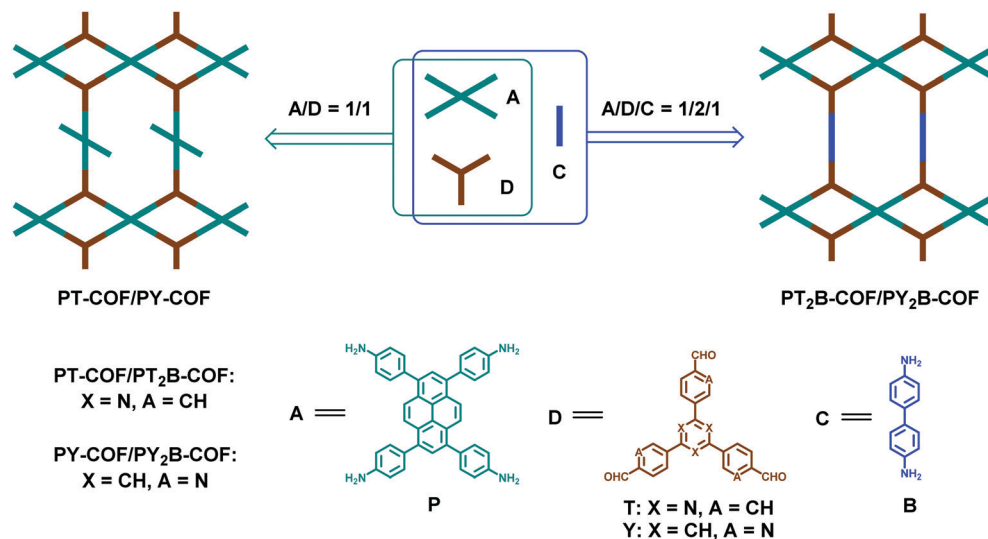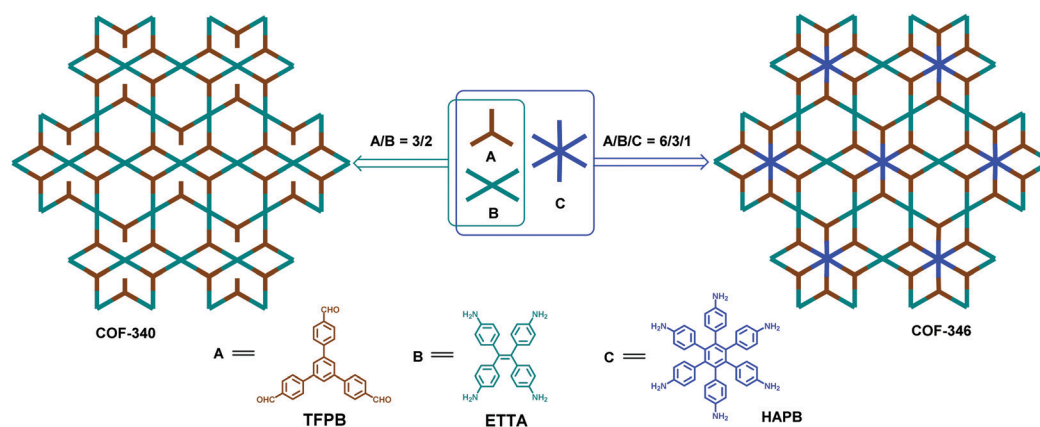

Fig. 18 Synthesis of **TTCOF-M**.[120]

3932 | Chem. Soc. Rev., 2020, **49**, 3920–3951

This journal is © The Royal Society of Chemistry 2020

Fig. 19 Synthesis of PT/PY-COFs and PT$_2$B/PY$_2$B-COFs.[121]

Fig. 20 Synthesis of **COF-340** and **COF-346**.[122]

ETTA (Fig. 20). Due to the unequal ratio of aldehyde and amine groups, **COF-340** was obtained as a hierarchically porous COF bearing aldehyde functional groups in its channels. Furthermore, the extraordinary combination of hexagonal hexamino-phenyl benzene (HAPB), tetragonal ETTA, and trigonal TFPB gave rise to an unprecedented heteropore COF with **tth** topology (**COF-346**) (Fig. 20). It possesses 3 kinds of vertices and 2 kinds of edges, representing a higher level of complexity of COF structures. By comparing the two typical examples with the combination of tetragonal and trigonal monomers, one can conclude that different feed ratios may afford totally distinct topological structures with different functional groups, which might lead to different applications. Except for [4+3] combination, other strategies such as the combination of appropriate hexatopic and tetratopic linkers can also be envisaged to produce sub-stoichiometric COFs. Therefore, optimizing the ratios of building blocks opens up a new way for the construction of COFs with hierarchical porosity. It is interesting that in these cases further formation of imine bonds of the unreacted amine or aldehyde groups was not observed, even various feed ratios of the

monomers were used. This is attributed to the steric hindrance provided by the pore environments for the functional groups.[122,123]

3.5 The combination of C_{2v}-symmetric vertexes and linear linkers

C_3-Symmetric monomers are the most widely used ones for the construction of COFs possessing homogeneous hexagonal pores. In this context, designing new monomers for the construction of heteropore COFs by modifying C_3-symmetric building blocks is handy and resourceful. Desymmetrizing a C_3-symmetric building block to a C_{2v}-symmetric one represents a nice strategy for such design.

3.5.1 Heteropore COFs with two different kinds of pores. Zhang and co-workers reported the first example of heteropore COFs constructed through the combination of C_{2v}-symmetric and linear building blocks.[124] Through changing the length of one branch of typical C_3-symmetric building blocks, they designed and synthesized two C_{2v}-symmetric monomers, 5-(4-formylphenyl)-isophthalaldehyde (FPPA) and 5-((4-formyl-phenyl)ethylene)-isophthalaldehyde (FPEPA). Using these two
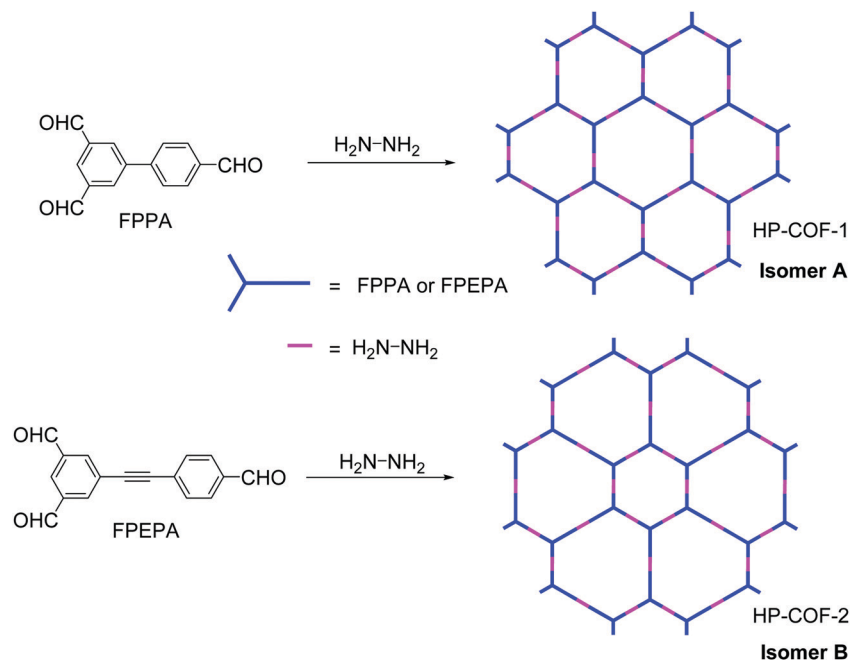
Fig. 21 Synthesis of **HP-COFs**.[124]

building blocks as the tritopic vertical monomers and hydrazine as the ditopic linear linker, two COFs (**HP-COF-1** and **HP-COF-2**) with two different kinds of hexagonal honeycomb pores were synthesized (Fig. 21). Since the combination of a C_{2v}-symmetric vertex and linear linker could theoretically generate two possible isomers (A and B) which exhibited almost the same XRD patterns, the structures of the as-prepared crystallites could not be assigned on the basis of their PXRD data. Fortunately, their structures could be identified through the comparison of the experimental PSD data with the theoretical pore sizes. It was found that while **HP-COF-1** adopted the form of isomer A (pore sizes: 1.06 and 1.96 nm), **HP-COF-2** was determined to possess the structure of isomer B (pore sizes: 1.26 and 1.89 nm) (Fig. 21).

Driven by the efficiency of the approach to construct hetero-pore COFs through the strategy of $[C_{2v} + C_2]$, in 2018, we designed a fluorescent monomer with C_{2v} symmetry to fabricate heteroporous fluorescent COFs.[125] By lengthening and doubling the linking sites at one branch of a C_3-symmetric monomer, a C_{2v}-symmetric monomer, 4′-(bis(4-formylphenyl)-amino)-[1,1′-biphenyl]-3,5-dicarbaldehyde (BABD), was produced. The condensation of BABD with 1,4-diaminobenzene and benzidine resulted in **COF-BABD-DB** and **COF-BABD-BZ**, respectively (Fig. 22). PXRD studies, theoretical simulations and PSD analysis revealed that the two COFs exhibited an unusual staggered stacking. Such partial stacking effectively suppressed the aggregation caused fluorescence quenching (ACQ) effect in the two COFs. As a result, both **COF-BABD-DB** and **COF-BABD-BZ** emit
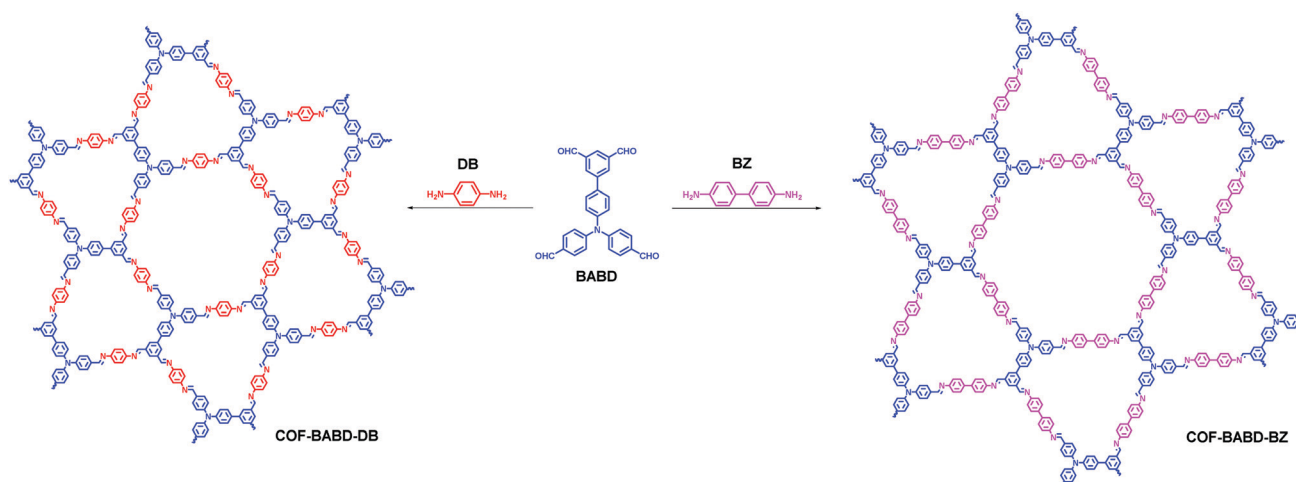
Fig. 22 Synthesis and structures of **COF-BABD-DB** and **COF-BABD-BZ**.[125]

3934 | *Chem. Soc. Rev.*, 2020, **49**, 3920–3951

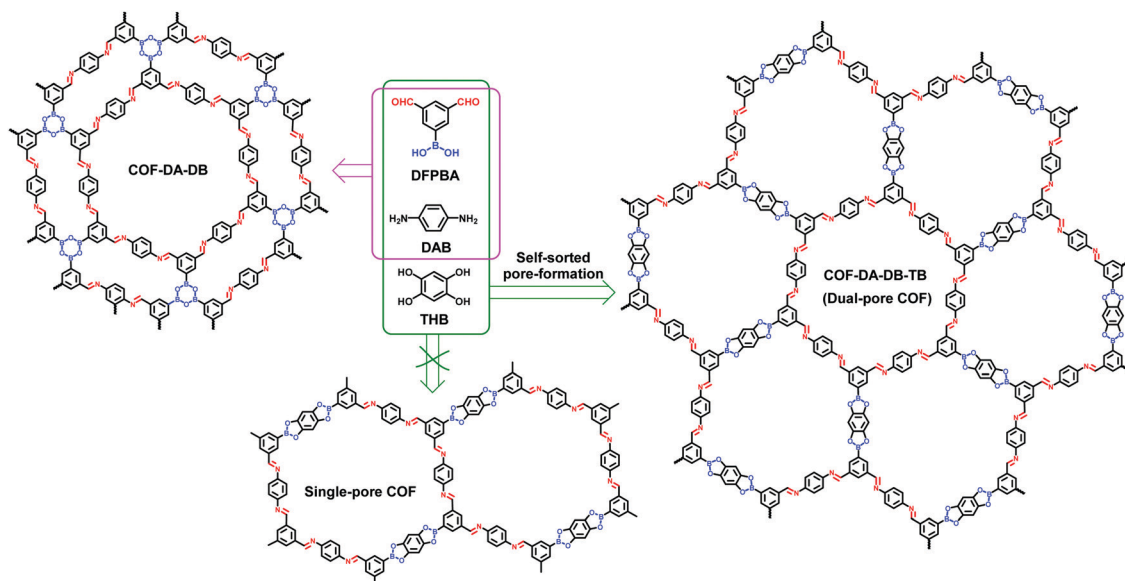This journal is © The Royal Society of Chemistry 2020

Fig. 23 Synthesis of **COF-DA-DB** and **COF-DA-DB-TB**, and the self-sorted pore formation leading to the dual-pore COF.[138]

strong green emission with high fluorescence quantum yields. Notably, the fluorescent heteropore COFs can be used as chemosensors to detect nitro aromatic compounds by means of fluorescence quenching. Both the COFs exhibit a high selectivity to TNP compared to 2,4-DNP (2,4-dinitrophenol), 2,4-DNT (2,4-dinitrotoluene), DNB (1,3-dinitrobenzene), NT (*p*-nitrotoluene), NB (nitrobenzene) and NP (*p*-nitrophenol). The Stern–Volmer constants for TNP sensing were estimated to be as high as 5.7×10^5 M^{-1} for **COF-BABD-DB** and 4.5×10^5 M^{-1} for **COF-BABD-BZ**, which are ten to hundred times larger than those obtained for other nitroaromatics examined. Moreover, they exhibit a rapid color change upon exposure to TNP, which allows the COFs to act as visual chemosensors for the naked-eye detection of TNP.

The orthogonal strategy, which involves the formation of at least two types of bonds in one system, is a method widely used for the construction of sophisticated supramolecular architectures.[126–132] Benefiting from its self-sorting behavior, such orthogonal bond formation has become one of the efficient tools to fabricate complicated and highly ordered structures.[133] Since 2015, the orthogonal strategy has also been used to fabricate COFs but most of them possess homogeneous porosity.[134–137] In 2018, we applied the orthogonal strategy to construct heteropore COFs.[138] 3,5-Diformylphenylboronic acid (DFPBA) was chosen as a bifunctional C_{2v}-symmetric building block to condense with 1,4-diaminobenzene (DAB) or DAB and 1,2,4,5-tetrahydroxybenzene (THB). The reactions generated two dual-pore COFs, **COF-DA-DB** and **COF-DA-DB-TB**, respectively (Fig. 23). It should be noted that theoretically the condensation of DFPBA, DAB and THB could afford two types of frameworks: single-pore and dual-pore COFs (Fig. 23). PXRD and PSD results provided unambiguous evidence for the formation of the dual-pore framework. In this COF, one type of pores consist of only imine bonds, which are connected by boroxine linkages to produce the other type of micropores. This thus led to an unprecedented self-sorted pore-formation in the polymerization process of the COF.

3.5.2 Heteropore COFs with three different kinds of pores.
In 2017, we reported a new strategy to fabricate a C_{2v}-symmetric monomer by combining vertex-truncation[139] and multiple-linking-site[140] strategies. Using this strategy, [1,1′:3′,1″-terphenyl]-3,3″,5,5″-tetracarbaldehyde (TPTCA) was designed by truncating a C_3-symmetric monomer which has two aldehyde groups at each end of the two branches. The condensation of TPTCA with linear monomers, 1,4-diaminobenzene and benzidine, led to the formation of two triple-pore COFs, **TP-COF-DAB** and **TP-COF-BZ**, respectively (Fig. 24).[141] Based on the results from PXRD, synchrotron small-angle X-ray scattering (SAXR), theoretical simulations, and PSD analysis, the structures of these two triple-pore COFs have been definitely determined. Furthermore, benefiting from the reversibility of dynamic covalent chemistry (DCC), *in situ* COF-to-COF transformation *via* linker exchange has been achieved. By heating **TP-COF-BZ** with excess 1,4-diaminobenzene under solvothermal conditions, **TP-COF-BZ** was completely transformed into **TP-COF-DAB** in 4 hours. Mechanistic studies show that the exchange of the linker is through an *in situ* framework-to-framework transformation process rather than a depolymerization–repolymerization process. This building unit exchange process can be used as a new methodology to synthesize COFs which are difficult or even impossible to synthesize through direct condensation of monomers. On the other hand, this strategy also provides a new avenue for the functionalization and property modification of COFs *via* structural doping. Recently, the practicality of this strategy for construction of COFs with unique structures has been demonstrated. For example, Horike and co-workers used a linker exchange strategy to fabricate COFs with core–shell hierarchical architectures.[91] Research studies conducted by Yaghi's group and Dichtel's group revealed that COFs with higher chemical stability or crystallinity, which were hard to access due to their inherently limited reversibility, could be fabricated through COF-to-COF transformation.[142,143] Furthermore, this
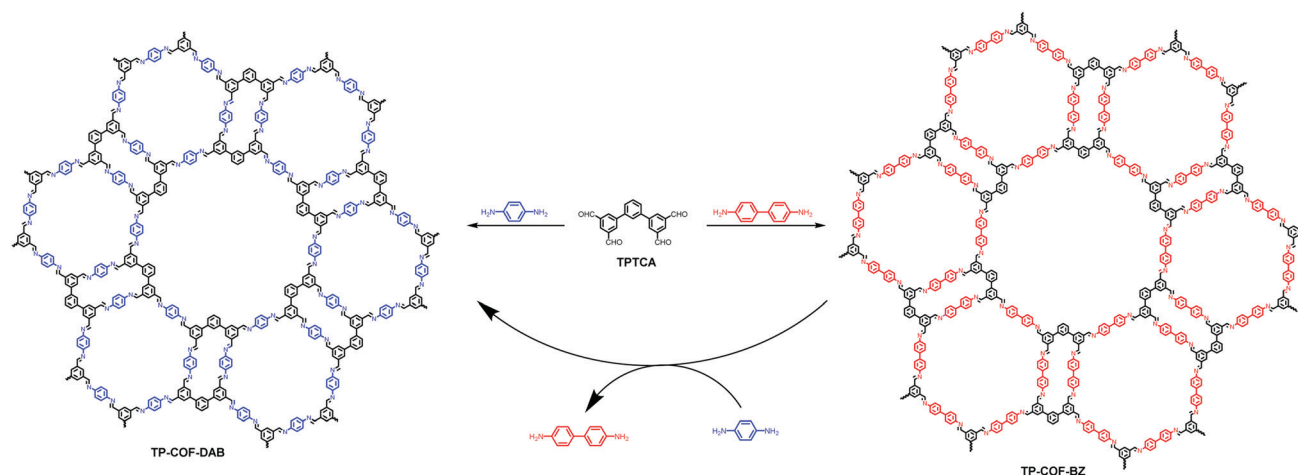
This journal is © The Royal Society of Chemistry 2020

Chem. Soc. Rev., 2020, **49**, 3920–3951 | **3935**

Fig. 24 Synthesis and structures of **TP-COF-DAB** and **TP-COF-BZ**, and the transformation from **TP-COF-BZ** to **TP-COF-DAB** *via* heterogeneous linker exchange.[141]

approach was also employed by Yan and co-workers to construct amino-functionalized imine-linked COFs, which are unattainable using a *de novo* method.[144] Very rectainabently, Han *et al.* have applied this approach for the structural transformation of 3D COFs and further realized dimensional transformation from 3D to 2D COFs.[145] These examples illustrate the great potential of this DCC-based building unit exchange strategy for constructing COFs which are difficult to obtain or unattainable under *de novo* synthetic conditions.

Undoubtedly, fabricating COFs with new topologies will increase the structural diversity of this class of crystalline porous materials. In 2019, Zhang and co-workers reported a 2D COF with a new topology by using a C_{2v}-symmetric benzimidazole-based tetraaldehyde building block (BITA).[146] Thanks to the judicious design of BITA, in which the four angles between the adjacent edges of the benzaldehyde groups are 60°, 90°, 90° and 120°, it meets the geometrical requirement for the tessellation of a 3.4.6.4 Archimedean tiling featuring

quadrilateral, triangular and hexagonal polygons (equivalent to a hexagonal tungsten bronze (**htb**) net topology). As a result, the condensation reaction of BITA with the diamine PDA afforded a triple-pore COF (**BITA-PDA COF**) with a unique **htb** net topology (Fig. 25). The PSD profile of the **BITA-PDA COF** exhibits three pore size distributions of around 1.0, 1.7, and 3.3 nm, which can be assigned to the trigonal, rectangular, and hexagonal pores, respectively, further confirming the formation of the triple-pore COF. The suspension of the **BITA-PDA COF** in DMF exhibits blue photoluminescence with a maximum emission band appearing at 432 nm upon being excited at 322 nm. Moreover, the COF suspension shows a specific fluorescence quenching effect toward Fe^{3+} ions among a number of metal cations including Cd^{2+}, Sn^{2+}, Mg^{2+}, Hg^{2+}, K^+, Li^+, Na^+, Al^{3+}, Sr^{2+}, Ni^{2+}, Ca^{2+}, Cu^{2+} and Co^{2+}, indicating its potential application in selective Fe^{3+} ion detection.

3.5.3 Heteropore COFs with four different kinds of pores. With the aim of constructing 2D COFs with highly complicated
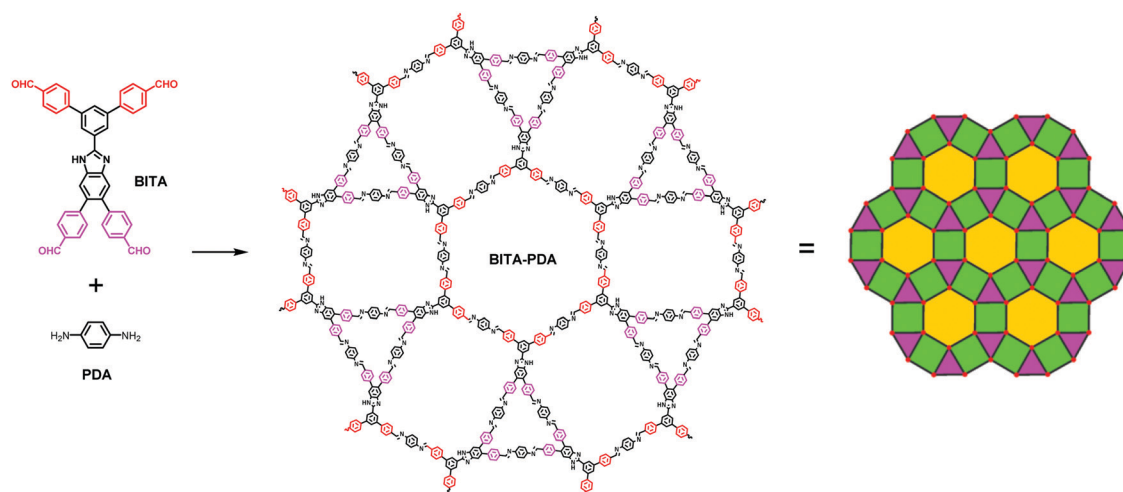

Fig. 25 The molecular structures of the tetraaldehyde precursor BITA and the diamine linker PDA, and the **BITA-PDA COF** with **htb** net topology.[146] Adapted from ref. 146 with permission from the Royal Society of Chemistry, copyright 2019.
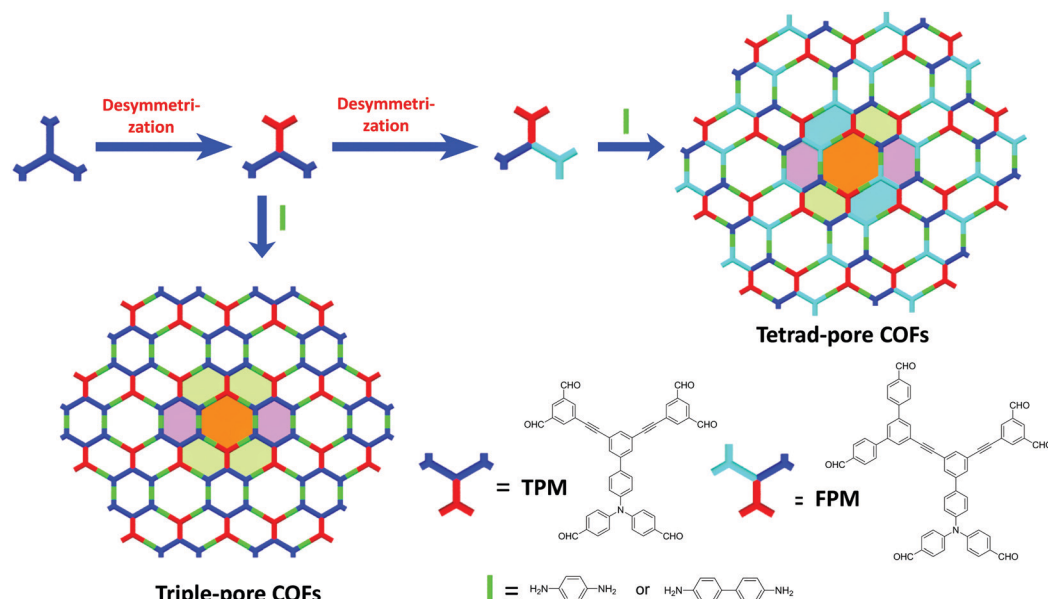
Fig. 26 Cartoon representation of the fabrication of triple-pore and tetrad-pore COFs.[147] Reproduced from ref. 147 with permission from Springer Nature, copyright 2019.

topological structures, we further developed a facile and general approach by combining multiple-linking-site[140] and desymmetrization[124] strategies simultaneously in 2019. In detail, a C_3-symmetric double-linking-site building block is initially selected as the primitive unit. Then, desymmetric operation is performed one or two times to give monomers with C_{2v}-symmetry (TPM) or inequilateral arms (FPM). While the condensation of TPM with linear 1,4-diaminobenzene or benzidine gave 2D COFs with three different kinds of pores (**Tri-COF-DAB** and **Tri-COF-BZ**), the use of FPM and 1,4-diaminobenzene or benzidine afforded tetrad-pore COFs (**Tetra-COF-DAB**, and **Tetra-COF-BZ**) which possess four different kinds of pores (Fig. 26).[147] PXRD results of these COFs revealed their crystalline structures. A transmission electron microscopy (TEM) study further confirmed the reliability of the structural identification of these COFs based on the PXRD analysis. All TEM images show clear lattice fringes, the distances between which are in good agreement with d-spacings of the (0 0 1) or (1 0 0) reflections of the predicted COF structures. Furthermore, clear reticular structures with approximately hexagonal pores were observed and the distances between two adjacent pores match well with the unit cell of a or c, respectively. These results provided compelling evidence for the formation of the predesigned COFs with complicated structures. The as-synthesized tetrad-pore COFs are the 2D COFs having the highest level of hierarchy and complexity reported so far, representing a successful step towards challenging the mathematically intricate tessellation patterns using synthetic chemistry.

3.6 The combination of C_{2v}- and C_3-symmetric building blocks

In addition to the $[C_{2v} + C_2]$ strategy used above, we reported a $[C_{2v} + C_3]$ approach to fabricate heteropore COFs in 2018.[148] In this work, the desymmetrization of C_3-symmetric building

blocks by shortening one branch or two branches leads to two C_{2v}-symmetric building blocks, $[1,1':3',1''$-terphenyl]$-4,4'',5'$-tricarbaldehyde (TPTA) and $[1,1'$-biphenyl]$-3,4',5$-tricarbaldehyde (BPTA), respectively. The condensation of TPTA or BPTA with a C_3-symmetric building block $4,4'$, $4''$-(1,3,5-triazine-2,4,6-triyl) trianiline (TTTA) led to the formation of heteropore COFs possessing two kinds of hexagonal micropores with different shapes and sizes (**COF-TTTA-TPTA** and **COF-TTTA-BPTA**, Fig. 27), respectively. Theoretically, the combination of such two symmetric monomers can also form two different framework isomers. However, different from the combination of $[C_{2v} + C_2]$ described above which gives rise two dual-pore COFs, the isomeric COFs obtained by the combination of $[C_{2v} + C_3]$ possess single-pore and dual-pore frameworks, respectively (Fig. 28). The two isomers display distinct PXRD patterns. This advantage enables their structures to be easily distinguished by PXRD data.

3.7 The combination of C_3-symmetric vertexes and linear linkers

3.7.1 Connection with the imine and olefin linkages. In most cases reported in the literature, the COFs synthesized through the combination of C_3-symmetric building blocks and linear linkers usually possess uniform hexagonal pores. However, with specific modifications, heterogeneous COFs could also be constructed through the $[C_3 + C_2]$ combination. In 2016, we developed a multiple-linking-site strategy by introducing double linking sites at each branch of a C_3-symmetric building block.[140] Without changing the symmetry, two new heteropore COFs were successfully fabricated through the $[C_3 + C_2]$ combination, a strategy which has been widely used to construct 2D COFs with homogeneous porosity. Using this strategy, the TPA-6CHO building block was designed and
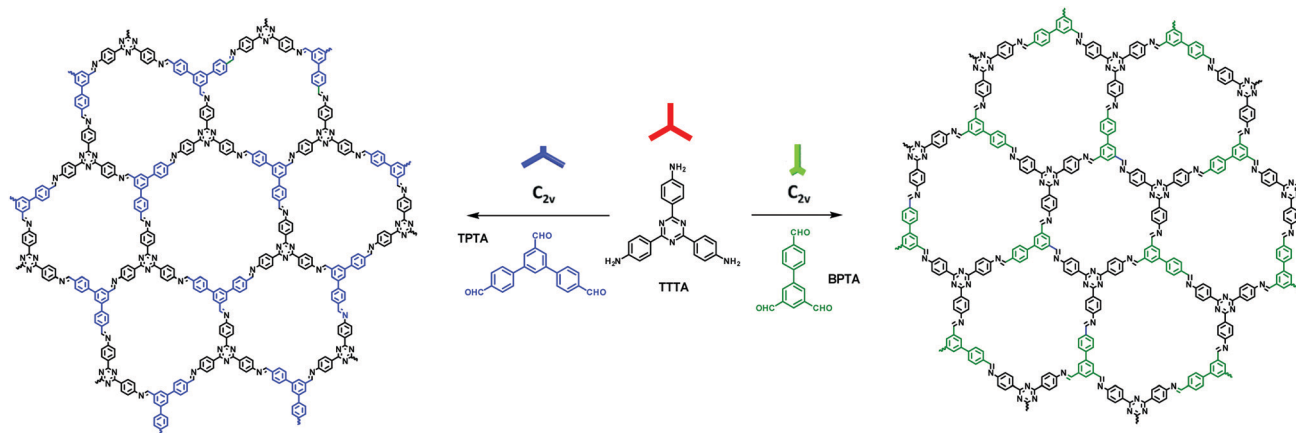
This journal is © The Royal Society of Chemistry 2020

Chem. Soc. Rev., 2020, **49**, 3920–3951 | **3937**

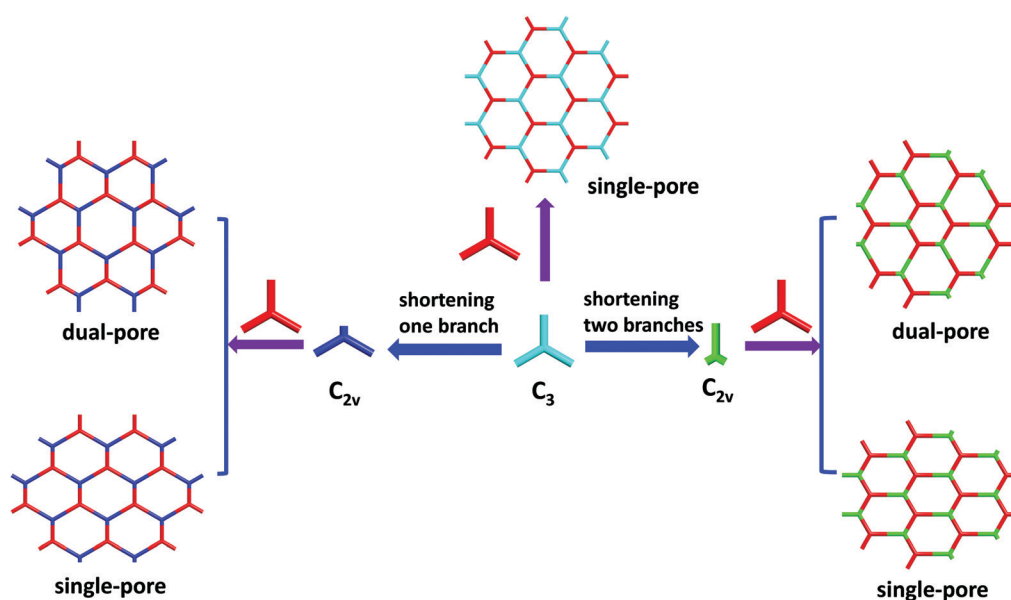**Fig. 27** Synthesis of **COF-TTTA-TPTA** and **COF-TTTA-BPTA**.[148]

Fig. 28 Framework isomers obtained through the combination of C_3- and C_{2v}-symmetric building blocks.[148] Reprinted from ref. 148 with permission from the Royal Society of Chemistry, copyright 2018.

synthesized, in which two aldehyde groups were introduced at each branch of the C_3-symmetric skeleton (Fig. 29). The condensation of TPA-6CHO with 1,4-diaminobenzene or benzidine gave heteropore COFs bearing two kinds of hexagonal pores with different sizes and shapes (**SIOC-COF-3** and **SIOC-COF-4**), which exhibit a unique hollow spherical morphology, uncommon staggered AB stacking of 2D sheets, and exceptionally high thermal stability. One advantage of this strategy is that it gives rise to only one type of framework without the formation of COF isomers and thus leads to the precise construction of heteropore COFs.

In 2016, we also reported a 2D COF (**HAT-COF**) containing two kinds of triangular micropores of different sizes (11.3 and 15.2 Å) by one-step condensation of a C_3-symmetric hexaazatriphenylene (HAT) derivative which has six amino groups outside and terephthalaldehyde (Fig. 30a).[149] This COF possesses

micropores with different chemical environments. Potentially, these two types of triangular micropores show different polarities which should lead to different properties and functions. In 2019, Jiang's group reported another 2D COF (**HFPTP-BPDA-COF**) which has the same topology as the **HAT-COF**, through the condensation of C_3-symmetric 2,3,6,7,10,11-hexakis(4-formyl-phenyl)triphenylene (HFPTP) with C_2-symmetric 1,1′-biphenyl-4,4′-diamine (BPDA) (Fig. 30b).[150] The **HFPTP-BPDA-COF** consists of two shape-persistent triangular pores with sizes of 12.7 and 15.5 Å respectively. The artificial 1D channel with a large aperture consists of three V-shaped nanogrooves at each corner and π-stacked walls that are covered by sequenced zigzag C–H units, which enable the COF to show precise size recognition of one atom difference. This dual-pore COF shows a fast uptake of Nile red (NR, 15.0 Å in size), but rejects 7-(diethyl-amino)-3-phenylcoumarin (DAPC) which has a molecule length
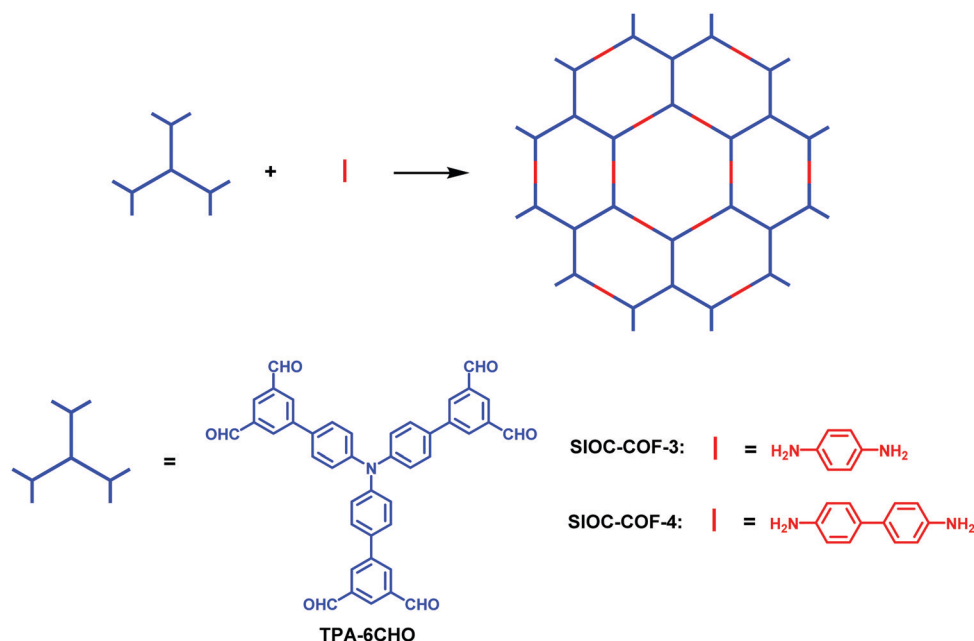
Fig. 29 Synthesis of COFs through the multiple-linking-site strategy.[140]

comparable to the pore aperture (15.5 Å) and coumarin 6 (C6) which is larger than NR by one atom. This is because when the NR molecules pass through the aperture, they rotate in the channels to adopt a pose with their π skeleton being parallel to the long axis of the channels. Subsequently, these NR molecules are confined at the corner nanogrooves. By contrast, the entry of guest molecules larger than the window will be blocked by the triangular aperture.

Another example of COFs having this kind of topology is reported by Feng *et al* in 2019. Using Knoevenagel condensation reaction, they synthesized a 2D sp²-carbon-linked conjugated polymer framework (**2D CCP-HATN**) through the condensation of 2,3,8,9,14,15-hexa(4-formylphenyl)diquinoxalino[2,3-a:2′,3′-c]-phenazine (HATN-6CHO) and 1,4-phenylenediacetonitrile (PDAN) (Fig. 30c, left).[151] Thanks to the sp² carbon–carbon linkages, this hexaazatrinaphthalene (HATN)-containing backbone is fully conjugated and exhibits high chemical stability. Benefiting from its stable shape-persistent framework and electrochemical redox-active HATN, **2D CCP-HATN** shows superior redox properties over its imine-linked COF analogue (**2D C=N HATN**, Fig. 30c, right). Furthermore, 2D CCP-HATN@CNT core–shell hybrids obtained through the in-situ growth of **2D CCP-HATN** on carbon nanotubes (CNTs) show a high capacity of 116 mA h g⁻¹ with superb cycling stability (91% capacity retention after 1000 cycles) and rate capability (82%, 1.0 A g⁻¹ *vs.* 0.1 A g⁻¹) and hence it is used as a cathode material for lithium-ion batteries (LIBs).

3.7.2 Connection with the triazine linkage. In addition to the multiple-linking-site strategy, the combination of common single-linking-site C_2-symmetric monomers and C_3-symmetric monomers could also afford heteroporous COFs in some special cases. This was illustrated by the synthesis of covalent triazine frameworks (CTFs) through a new approach reported

by Tan *et al.*[152] A CTF was firstly reported by Thomas *et al.* in 2008 with 1,4-dicyanobenzene as a monomer.[153] Due to their excellent stability, CTFs have been of interest to materials scientists. However, the harsh conditions (in molten $ZnCl_2$ at 400 °C) of ionothermal synthesis usually cause the partial carbonization of the materials and thus limit their applications. In 2017, Tan and co-workers developed a new method to synthesize CTFs under milder conditions *via* a condensation reaction between aldehyde and amidine dihydrochloride, which involves Schiff base reaction followed by Michael addition.[152] Due to the utilization of two types of monomers with different functional groups, the combination of two building blocks with different lengths or symmetries leads to dual-pore COFs (Fig. 31), which provides a novel strategy to synthesize hierarchically structured 2D COFs. Moreover, this method leads to the production of CTFs with a scale up to gram quantities. These CTFs are found to be promising photocatalysts for sacrificial photocatalytic hydrogen evolution with a maximum rate of 2647 μmol h⁻¹ g⁻¹ under visible light and also show good performance in sodium-ion battery applications after pyrolysis.

3.8 The combination of two C_2-symmetric building blocks

In some cases, the combination of $[C_2 + C_2]$ may also give rise to heteropore COFs such as the CTFs constructed from C_2-symmetric amidines and C_2-symmetric aldehydes illustrated above (Fig. 31d).[152] Another method to fabricate heteropore COFs through the combination of $[C_2 + C_2]$ is to use at least one kind of C_2-symmetric building block bearing additional branches, for example, possessing multiple linking sites or different types of linking sites. In 2017, we designed and synthesized a C_2-symmetric building block, 4,4″-bis(bis(4-formylphenyl)amino)-[1,1′:4′,1″-terphenyl]-2′,5′-dicarbaldehyde (BFATD), which is a hexa-aldehyde monomer through putting two aldehyde groups

This journal is © The Royal Society of Chemistry 2020

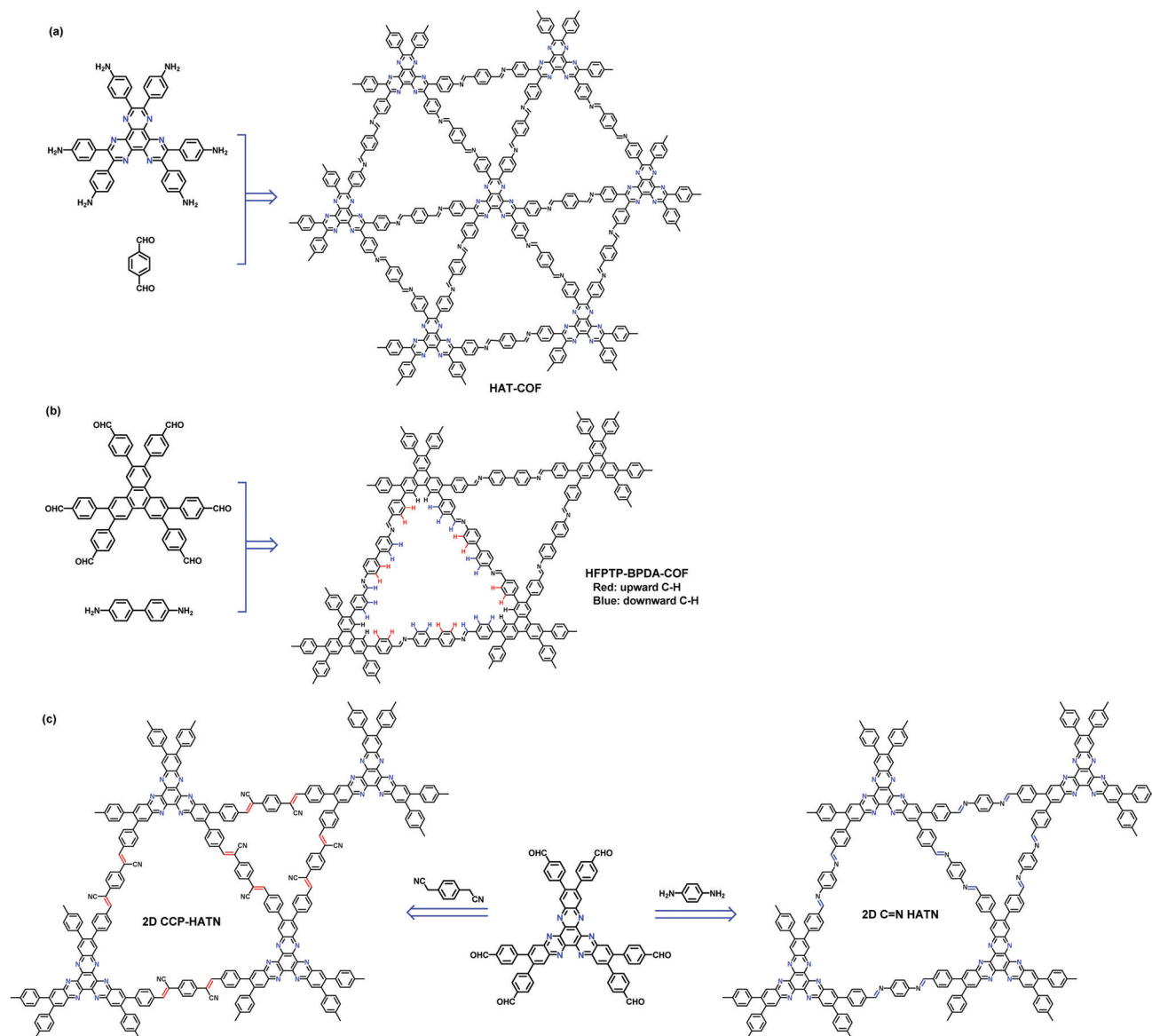*Chem. Soc. Rev.*, 2020, **49**, 3920–3951 | **3939**

Fig. 30 Synthesis and structures of (a) **HAT-COF**, (b) **HFPTP-BPDA-COF**, and (c) **2D CCP-HATN** (left) and **2D C═N HATN** (right).[149−151]

in the middle of the backbone of a D_{2h}-symmetric tetra-aldehyde.[154] The condensation of the BFATD monomer with C_2-symmetric phenylenediamine affords a 2D heteropore COF (**SIOC-COF-7**), which contains deformed hexagonal pores and quadrilateral pores (Fig. 32). PSD analysis reveals that the sizes of these two kinds of pores are around 5.0 and 11.8 Å, respectively. It is worth noting that **SIOC-COF-7** exists as a hollow microsphere with diameters being one to two micrometers and the shell thicknesses being hundreds of nanometers. Surprisingly, **SIOC-COF-7** exhibits an ultra-high iodine uptake capacity of 481 wt%. This result can be attributed to two aspects. Firstly, the abundant aromatic rings and the well-ordered network of the COF are favorable for iodine enrichment. Secondly, iodine is not only adsorbed in the channels of the COF, but it is also encapsulated in the hollow cavity of the COF microspheres. Being the first example of COFs used for iodine adsorption, this research has explored a new

application of COFs. Moreover, the special morphology suggests that COF-based hollow nanomaterials have great potential for applications in substance capture, storage and delivery.

In 2019, Chen and co-workers reported an innovative two-in-one strategy to construct COFs based on a C_2-symmetric monomer, which is a variation of D_{2h}-symmetric building blocks.[155] Using this strategy, two different types of functional groups (*i.e.*, formyl and amino groups) are integrated into one molecule to afford a bifunctional C_2-symmetric monomer. Therefore, COFs can be prepared by the self-condensation of such bifunctional monomers. In this work, 1,4-bis(4-formyl-phenyl)-2,5-bis((4-aminophenyl)ethynyl) benzene (BFBAEB) and 1,6-bis(4-formylphenyl)-3,8-bis((4-aminophenyl)ethynyl)pyrene (BFBAEPy) were designed and synthesized. Both bifunctional building blocks with different substituted arm lengths preferred to form dual-pore COFs with **kgm** topology (Fig. 33). An advantage of this two-in-one strategy is that it could realize

3940 | *Chem. Soc. Rev.*, 2020, **49**, 3920−3951

This journal is © The Royal Society of Chemistry 2020

(a)

(b)

(c)

(d)
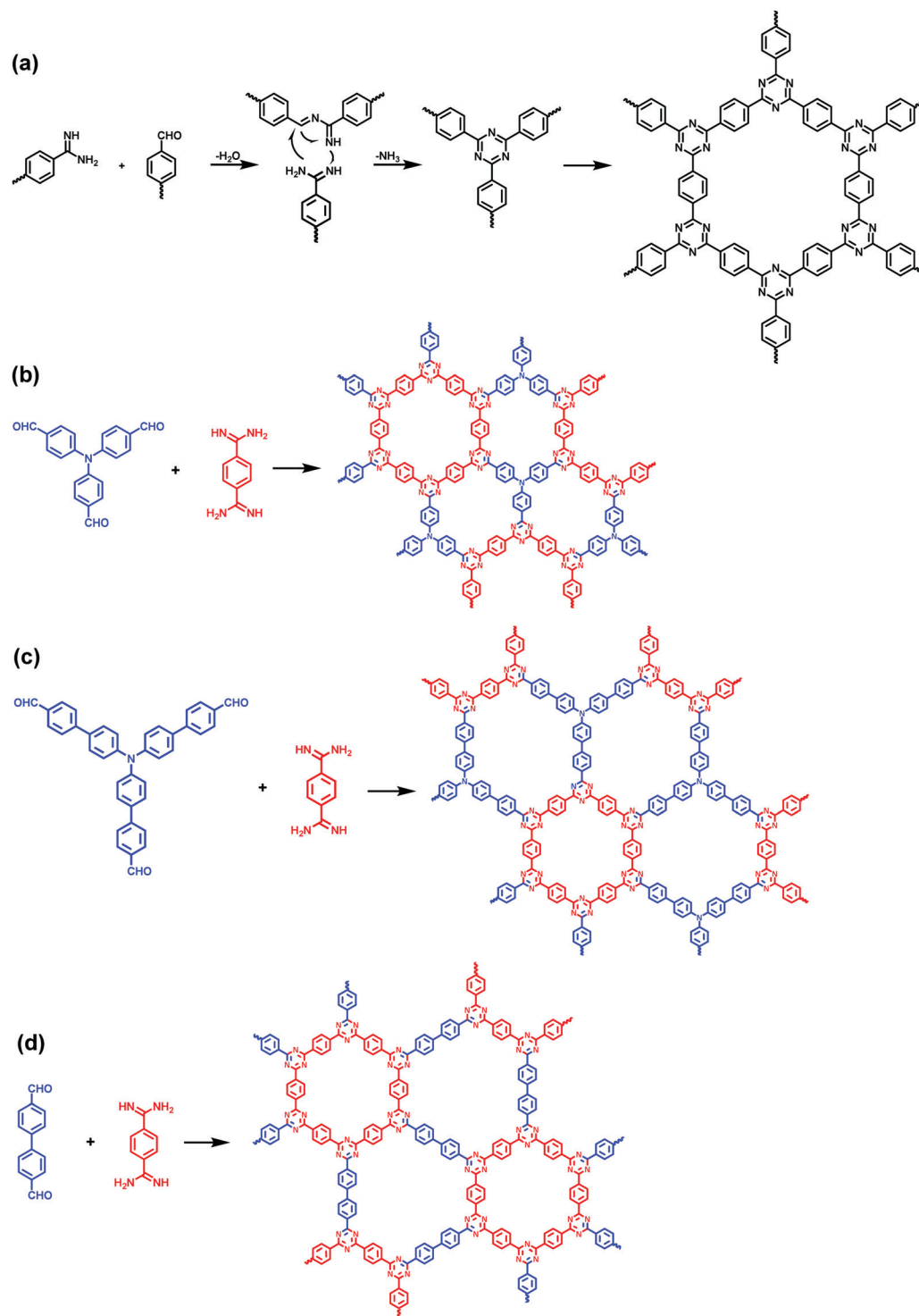
Fig. 31 Synthesis and structures of the CTFs.[152]

the construction of highly crystalline COFs in various solvents, exhibiting excellent solvent adaptability.

3.9 Macrocycles as promising building blocks to construct heteropore COFs

With the development of COFs, cyclic building blocks have also been employed as monomers (usually used as vertexes) for the construction of COFs (Fig. 34). The use of these interesting building blocks undoubtedly improves the structural diversity of COFs and integrates different functions into frameworks. The use of cyclic building blocks for the construction of 2D COFs can be traced back to 2013, when Jiang and co-workers reported the synthesis of star-shaped 2D COFs by the condensation of 9,10-hydroxyphenanthrene cyclotrimer (HPCT) with

This journal is © The Royal Society of Chemistry 2020

Chem. Soc. Rev., 2020, 49, 3920–3951 | 3941
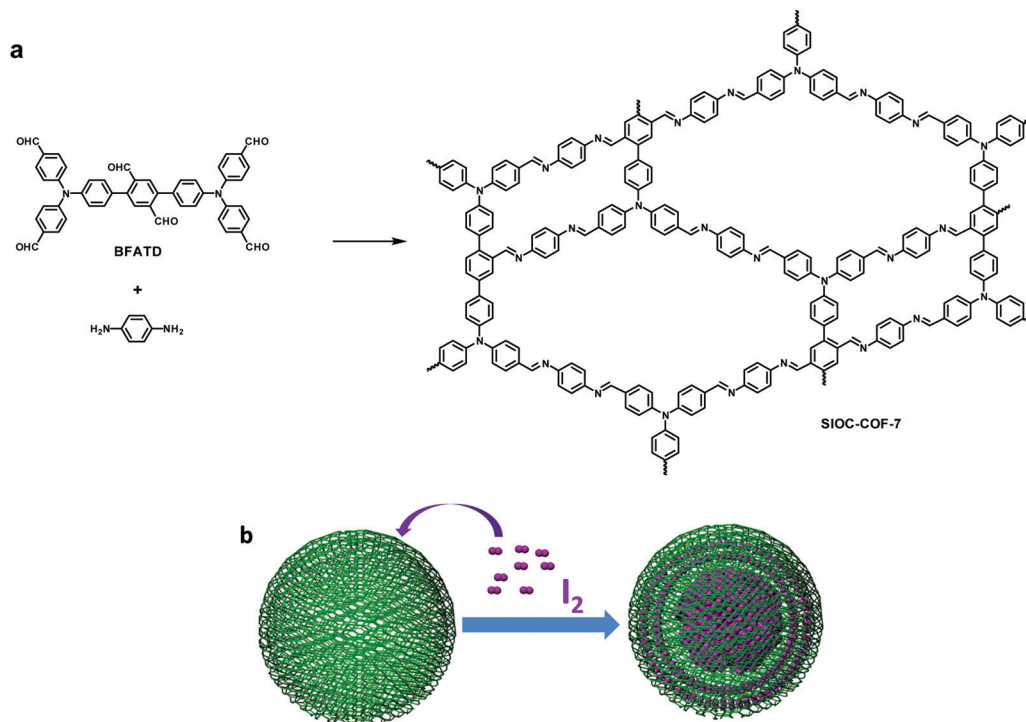
Fig. 32 (a) Synthesis and structure of **SIOC-COF-7** and (b) cartoon illustration of iodine capture in the hollow COF microsphere.[154] Adapted from ref. 154 with permission from the Royal Society of Chemistry, copyright 2017.
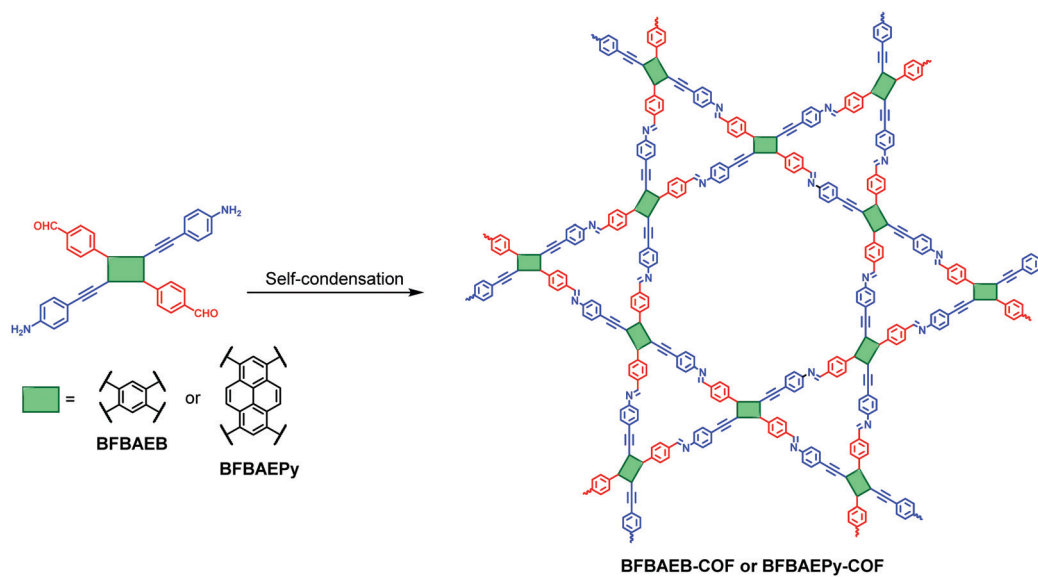
Fig. 33 Synthesis and structures of heteropore COFs through the two-in-one strategy.[155] Adapted from ref. 155 with permission from American Chemical Society, copyright 2019.

diboronic acids (Fig. 34).[156] Although these COFs exhibit homogeneous porosity as the internal cavity of HPCT (around 3.0 Å as estimated by CPK modeling) is too small to be identified as a pore, this approach can be developed as a general method to fabricate heteropore COFs by using macrocycles with cavities large enough to provide additional porosity. This was further investigated by Zhang's group[157] and McGrier's group[158]

through the use of three macrocyclic monomers AEM-1(DBA[12]), AEM-2, and DBA[18], which have interior voids of 0.4, 0.58 and 0.5 nm, respectively (Fig. 34).[157,158] For this macrocycle-to-framework strategy, polycondensation reactions of 1,4-benzenediboronic acid (BDBA) with these macrocycles under solvothermal conditions afforded the expected crystalline COFs. However, only the mesopores, with pore sizes ranging from

3942 | Chem. Soc. Rev., 2020, 49, 3920–3951

This journal is © The Royal Society of Chemistry 2020

Fig. 34 Synthesis of 2D COFs from cyclic building blocks.[156–158]

3.2 to 3.8 nm, were observed by PSD analysis. The micropores contributed by the intrinsic cavities of the shape-persistent macrocycles were not identified, which was attributed to the possible defects and offset stacking of the COF layers.[157,158]

To further increase the size of the internal cavity of macrocyclic building blocks, Zhang and co-workers developed a square-shaped macrocycle with non-collapsible interna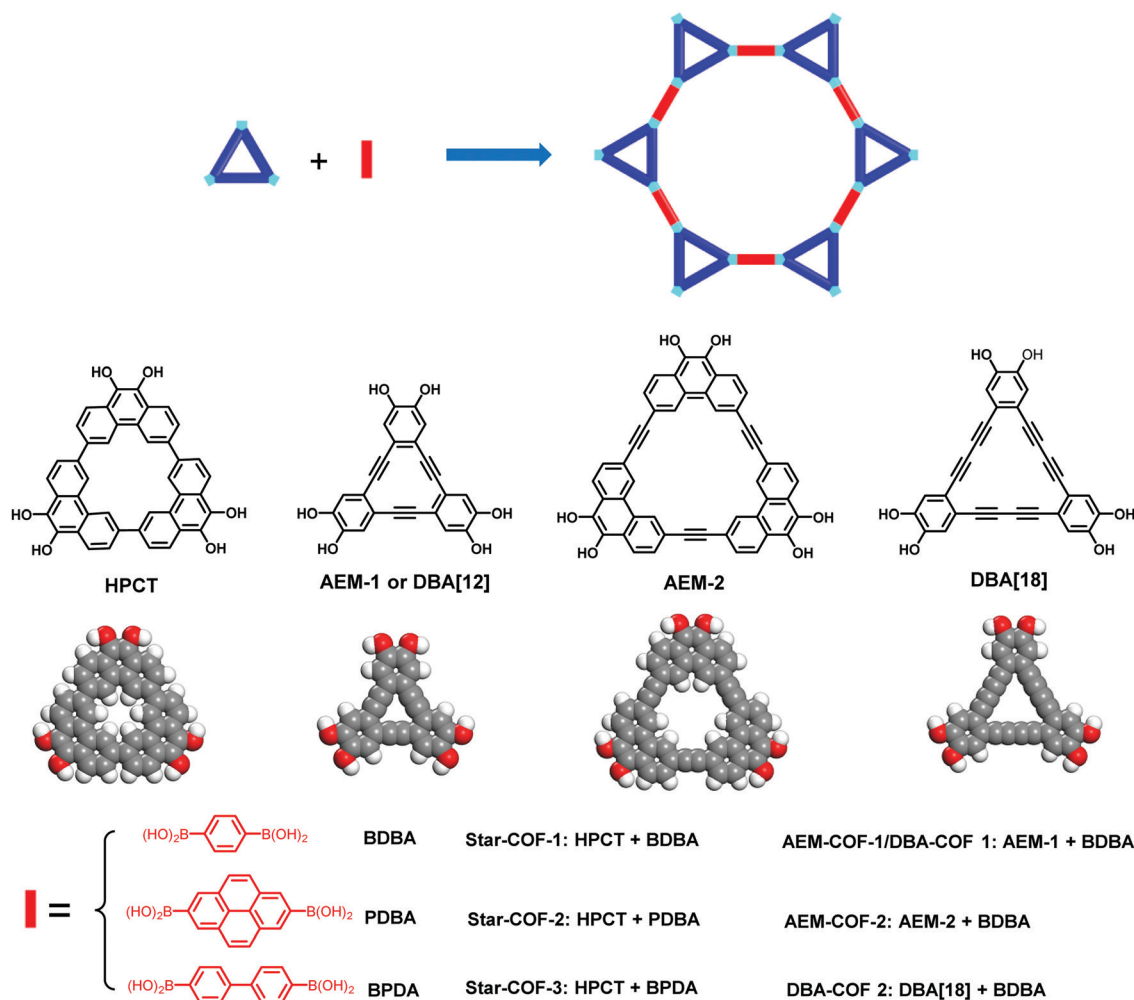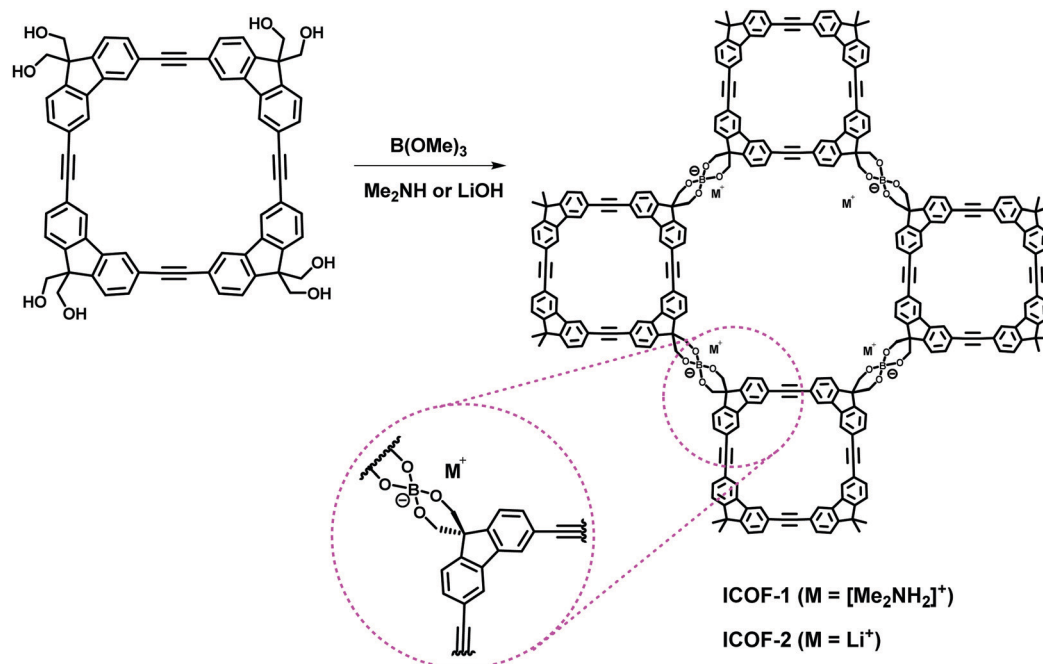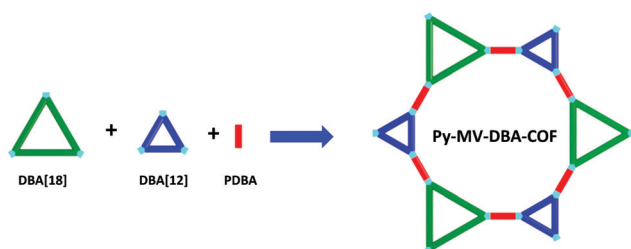l cavities of about 9 Å (estimated by CPK modelling), from which two spiroborate-linked ionic COFs (**ICOF-1** and **ICOF-2**) were constructed (Fig. 35).[159] However, due to the complex diffraction patterns and the limited quality and resolution of the PXRD data, their crystal structures were unable to be determined and only 2D framework structures were proposed. Moreover, no micropores below 1 nm were detected by the PSD analysis of the two ICOFs, which might be ascribed to the low crystallinity of the materials. Nevertheless, both the ICOFs exhibited excellent uptake of H_2 (up to 3.11 wt%, 77 K, 1 bar) and CH_4 (up to 4.62 wt%, 273 K, 1 bar). Benefiting from the presence of permanently immobilized ion centers in ionic borate linkages, the ICOFs were able to transport lithium ions at room temperature. **ICOF-2** showed a room temperature conductivity of 3.05×10^{-5} S cm^{-1} and an average Li$^+$ transference number

value of 0.80 ± 0.02 (measured by the Bruce–Vincent–Evans method), which indicated its potential application as a solid lithium electrolyte or separator for lithium batteries.

Similar to the mixed linker strategy we developed for the construction of triple-pore COFs,[96] McGrier and co-workers reported a mixed vertex strategy to fabricate a multiple component COF (**Py-MV-DBA-COF**) by using both DBA[12] and DBA[18] as vertexes of the COF (Fig. 36).[160] As a result, a heterogeneous distribution of the macrocycles in the COF was achieved. In addition to the **Py-MV-DBA-COF**, two-component COFs, **Py-DBA-COF 1** and **Py-DBA-COF 2**, were also synthesized. Similar to other macrocycle-based COFs previously reported, only large mesopores were observed in their PSD profiles. Interestingly, these COFs exhibited unique luminescence properties in the solid state, with **Py-DBA-COF 2** showing a blue-greenish luminescence color, while **Py-DBA-COF 1** and **Py-MV-DBA-COF** displaying yellow luminescence under UV radiation, suggesting that the DBA[12] units dominated the excited-state properties of the **Py-MV-DBA-COF**.

To make the macrocycle-to-framework strategy more efficient, using macrocycles with larger internal cavities is a good choice. Although synthesis of such organic building blocks is sometimes difficult compared to the noncyclic ones, these strategies have the

This journal is © The Royal Society of Chemistry 2020

Chem. Soc. Rev., 2020, **49**, 3920–3951 | **3943**

Fig. 35 Synthesis of ICOFs.[159]

ICOF-1 (M = [Me$_2$NH$_2$]$^+$)
ICOF-2 (M = Li$^+$)

Fig. 36 Construction of the **Py-MV-DBA-COF** containing a heterogeneous distribution of DBAs.[160]

advantage of avoiding the polymorphism issue which usually arises when the noncyclic building blocks are used to fabricate 2D COFs with hierarchical structures.

As demonstrated in this section, heteropore COFs exhibit a much more structural diversity than COFs with uniform pores. However, design strategies for their construction are quite limited, among which the $[D_{2h} + C_2]$ approach stands out from the others. Differing from their single-pore congeners, there will be many combinations for hetropore COFs to integrate different pores into one skeleton. This creates a large number of potential structures waiting to be explored. To accelerate the experimental exploration of heteropore COFs with new topological structures, developement of new design principles is essential.

4 Superior performance and unique applications of heteropore COFs

Over the past several years, a variety of heteropore COFs have been reported and many of them have been found to show various applications. However, their applications, such as adsorption, catalysis, and sensing, as described above, have not yet gone beyond the applications explored for COFs with homogeneous porosity. Compared with single-pore COFs, heteropore COFs exhibit unique structural features in that different types of pores are integrated into one framework, which should endow them with some specific properties and applications that single-pore COFs do not have. Although the exploration of such properties and applications is just in its incipient stage, heteropore COFs have indeed been recognized to exhibit superior performance and unique applications in some aspects. In 2019, Ma and co-workers found that the heteropore COFs exhibited advantages over single-pore COFs as hosts for enzymes to catalyze organic reactions.[161] According to their previous reports, the performance of an enzyme could be systematically optimized by changing the pore environment of the host COFs.[162] In the case of the lipase PS, the hydrophobic channels in the COFs can improve its activity by opening a lid near the active site. Although such COF–enzyme systems can prevent the enzymes from deactivation and exhibit higher catalytic activities than the free enzymes, there is still some room for improvement. Firstly, the enzymes will completely or partially block the pores of COFs. Secondly, flux rates for reagents and products are slow. To solve these problems, they designed a dual-pore kagome COF (**COF-ETTA-EDDA**) formed through the condensation of ETTA and 4,4′-(ethyne-1,2-diyl)-dibenzaldehyde (EDDA) (Fig. 37a). Both PXRD and PSD analyses revealed the formation of a dual-pore COF with diameters of 13.9 and 38.5 Å for the triangular micropores and hexagonal mesopores, respectively. In their design, the large hexagonal pores were used to encapsulate enzymes which thus serve as catalytic spaces, while the small triangular pores were utilized
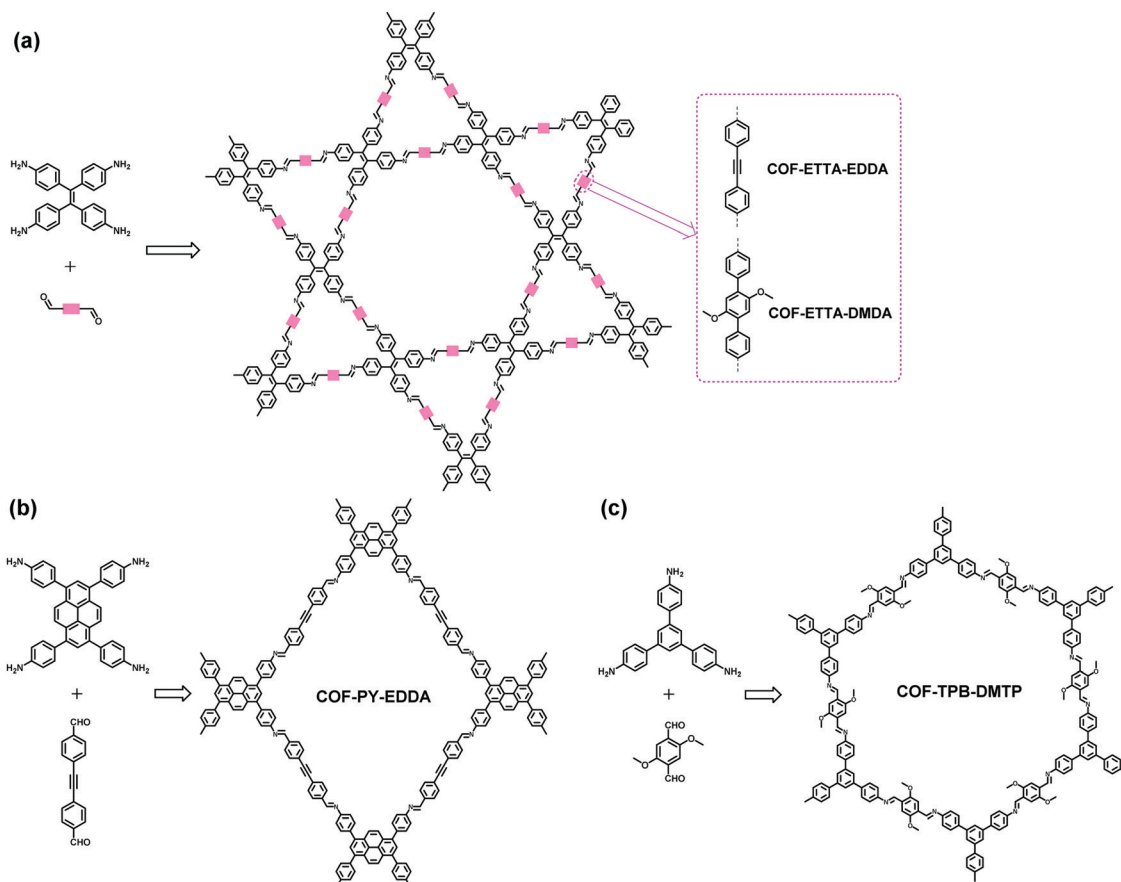
3944 | *Chem. Soc. Rev.*, 2020, **49**, 3920–3951

This journal is © The Royal Society of Chemistry 2020

Fig. 37 Synthetic schemes of (a) **COF-ETTA-EDDA** and **COF-ETTA-DMDA**, (b) **COF-PY-EDDA**, and (c) **COF-TPB-DMTP**.[161]

as transport channels to transfer reagents and products. After immobilizing the enzyme lipase PS, the kinetic resolution of racemic secondary alcohols was chosen to evaluate the catalytic performance of lipase@**COF-ETTA-EDDA**. In order to evaluate the effect of the hierarchically porous structure of the dual-pore COF on the catalytic properties of the enzyme, a control experiment was conducted by using a single-pore COF (**COF-PY-EDDA**) with the pore aperture and environment similar to those of the hexagonal mesopores in **COF-ETTA-EDDA** for comparison (Fig. 37b). Both lipase@COFs showed drastically enhanced activities compared to the free enzyme. Surprisingly, with the same enzyme content, lipase@**COF-ETTA-EDDA** exhibited approximately 1.5 times higher improvement in catalytic activity than lipase@**COF-PY-EDDA**. Kinetic experiments showed that this difference was mainly attributed to mass transfer as the mesoporous channels in **COF-PY-EDDA** were occupied by the enzyme. More control experiments were performed on another dual-pore COF material (**COF-ETTA-DMDA**) and its single-pore analogue (**COF-TPB-DMTP**) (Fig. 37a and c). Both COFs have similar hexagonal pores but single-pore **COF-TPB-DMTP** has a larger surface area (the BET surface area of **COF-ETTA-DMDA** is 952 $m^2\ g^{-1}$, while that of **COF-TPB-DMTP** is 1740 $m^2\ g^{-1}$). In spite of the higher surface area, the corresponding biocomposite of single-pore **COF-TPB-DMTP** did not display a superior catalytic performance compared to that of dual-pore **COF-ETTA-DMDA**.

This result further demonstrates the use of heteropore COFs as host materials for enzymatic catalysis, clearly revealing the superiority of the hierarchical porosity of heteropore COFs.

Another example demonstrating the unique properties and applications of heteropore COFs has been reported by our group very recently, in which an unprecedented application of COFs has been explored.[163] The idea is to fabricate organic nanotubes through selectively disassembling dual-pore COFs. While 2D COFs are generally regarded as porous materials containing highly ordered nanochannels, from a different perspective, they can also be viewed as orderly bundled nanotube arrays. In this context, selective bond-breaking in 2D COFs may provide a chance to obtain isolated nanotubes through disassembling the "bundled nanotubes". To realize this design, 2D heteropore COFs are feasible precursors, because their hierarchical structures provide selectivity for bond-breaking. By contrast, bond-breaking in 2D COFs with homogeneous porosity will lead to the deconstruction of the channels due to their totally identical pore structures. The second prerequisite of the design is that linkages in different kinds of pores must exhibit different stabilities to accomplish selective bond-breaking. To meet these requirements, a dual-pore COF (**COF-OEt**) constructed through orthogonal reactions, here hydrazone formation and trimerization of boronic acids, was designed and synthesized as the precursor COF by the condensation
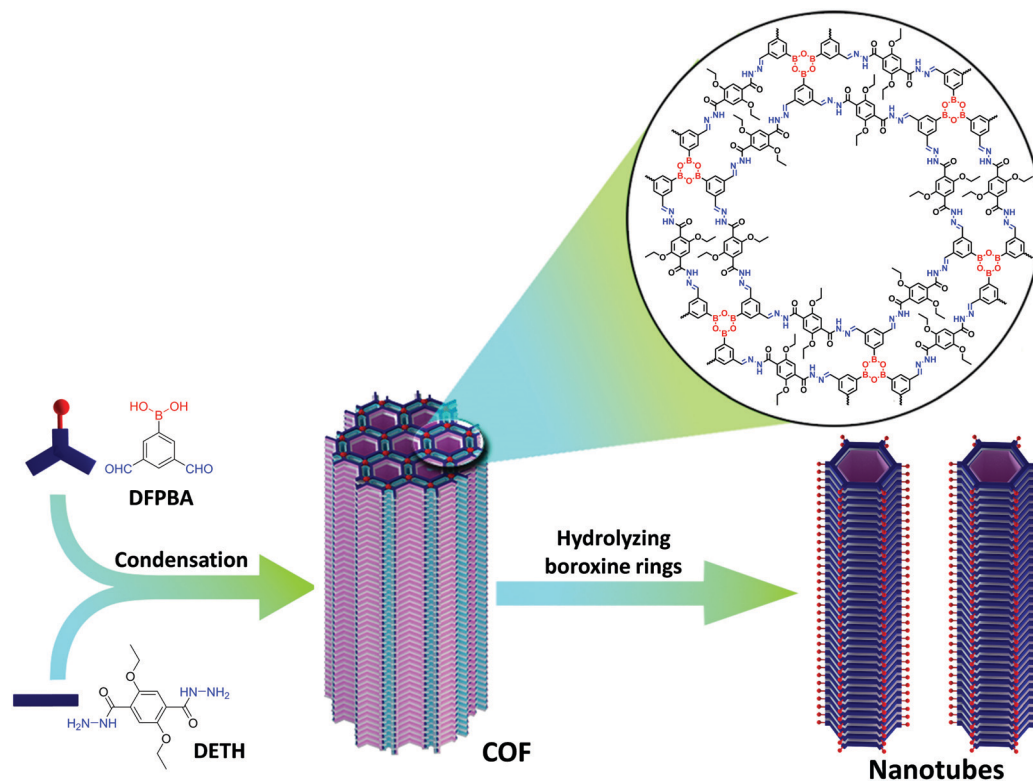
This journal is © The Royal Society of Chemistry 2020

Chem. Soc. Rev., 2020, **49**, 3920–3951 | **3945**

Fig. 38 Schematic illustration of the fabrication of nanotubes through selectively hydrolyzing a 2D heteropore COF.[163] Reproduced from ref. 163 with permission from American Chemical Society, copyright 2020.

of DFPBA and 2,5-diethoxyterephthalohydrazide (DETH) (Fig. 38). **COF-OEt** possesses two different types of pores with one being all-hydrazone-linked nanopores and the other is formed by connecting the former ones with boroxines. Thanks to the dramatic difference between the hydrazine and boroxine linkages in the stability against hydrolysis, upon suspending the COF in aqueous hydrochloride acid solutions, the boroxine rings were completely hydrolyzed, while the hydrazine units stayed untouched. By this way, nanotubes with a predictable diameter and shape could be obtained after the selective disassembly of **COF-OEt**. Another isostructural dual-pore COF (**COF-OAl**) was also synthesized by the condensation of DFPBA and 2,5-bis-(allyloxy)terephthalohydrazide (BATH). The allyoxyl groups in the adjacent layers were further cross-linked by alkene meta-thesis reaction. Hydrolysis of the COF after cross-linking gave rise to organic nanotubes with excellent stability. They could withstand ultrasonic treatment. For the nanotubes fabricated from **COF-OEt**, ultrasonic treatment led to their breakdown. This work has explored an innovative application of COFs, which also led to a top-down approach for the designable and precise fabrication of organic nanotubes.[164] On the other hand, this work also nicely illustrates a certain superiority of heteropore COFs. While they can be used as porous materials to do the jobs what the single-pore COFs do, they do have exclusive applications for which single-pore COFs cannot be competent. In addition to the fabrication of organic nanotubes, this strategy should also be useful for the synthesis of macrocycles with nanoscale cavities, which are usually hard to access *via* direct organic synthesis.

These two examples clearly demonstrate the advantages of heteropore COFs over single-pore COFs in certain applications, which is encouraging and will undoubtedly attract more attention from researchers in different fields. Inspired by these exciting achievements, we envisage that more and more intriguing properties and unique applications offered by heteropore COFs will be explored in the near future.

5 Conclusions and perspectives

In this article, we have provided a comprehensive review of the pore engineering of 2D COFs, with a focus on those exhibiting hierarchical porosity. Since the emergence of heteropore COFs in 2014, a growing number of heteropore COFs have been synthesized, using the design strategies developed for them. Meanwhile, most of them have been found to show applications in many fields as the COFs with homogeneous porosity do, suggesting their versatile application as porous materials. A distinctive characteristic of heteropore COFs lies in their hierarchical framework structures, which not only create different pore environments, but also offer a great opportunity for the differential pore engineering of different types of pores in one COF. This advantage may lead to many innovative functions and applications, for example, the simultaneous encapsulation of different guest molecules in different kinds of pores, integrating different functional units into different kinds of pores to fabricate multifunctional devices, creating different

3946 | *Chem. Soc. Rev.*, 2020, **49**, 3920–3951

This journal is © The Royal Society of Chemistry 2020

functional areas to undertake different jobs, and many others related to their hierarchical structures. Thanks to their unique structural characteristics, heteropore COFs have already been revealed to exhibit superior performance in catalysis as different types of pores execute different functions. Moreover, heteropore COFs have recently been explored for an exclusive application that COFs with uniform pores cannot achieve.[163] However, despite much progress being made over the past 5 years, there are still new lands to be explored and challenges to be addressed. In addition to the general issues faced by the whole COF family,[80–83] there are also some aspects specific to heteropore COFs. The first one is that design strategies for them are still quite limited, which leads to limited topological structures for this emerging class of porous organic materials. To increase the diversity of their topology, novel building blocks with symmetries other than the ones summarized in Section 3 or different combinations of building blocks need to be developed. On the other hand, exploring new linkage chemistry should be another way to reach this goal, as new linkages can also lead to new topologies even with building blocks bearing a symmetry commonly used for the construction of other topologies. A nice example is the **cpi** net of the aminal-COFs constructed from the combination of D_{2h}- and C_2-symmetric building units,[119] which previously has been a general approach to synthesize COFs with **kgm** topology. Thirdly, COFs with much higher hierarchical structures deserve to be further developed. This is not just to challenge the complicated architectures in Nature using synthetic chemistry, but also to establish a deeper understanding of the design principles of COFs and to create new opportunities for exploring novel properties and applications.

The second challenge that this field will face in the near future is the structural elucidation of complicated hierarchical COFs. As mentioned in Section 2, the structural elucidation of heteropore COFs also follows the method widely used for COFs with homogeneous porosity, that is, the combination of computational simulations, PXRD, and porosity analysis. However, these data might be insufficient to elucidate framework structures with increased complexity. In some cases, isomeric frameworks might exhibit similar or even the same diffraction patterns. As a result, their structures are hard to distinguish or cannot be distinguished by PXRD. On the other hand, PSD analysis, which is used to identify the existence of the predicted pores, might fail to provide valid information for certain structures, especially for those with close pore widths or irregular pore shapes. Moreover, with the increase of the structural complexity of heteropore COFs, it might be hard to select a suitable kernel/pore model to generate a valid PSD profile.[147] In this context, advanced techniques are highly desired for the accurate characterization of hierarchically porous COFs. Recently, single-crystal X-ray analysis and continuous rotation electron diffraction, which provide a resolution as high as 0.83 angstroms, have been used to determine the crystal structures of COFs.[21,165,166] Moreover, TEM should also be a powerful technique for the characterization of these hierarchical materials. With resolution being high enough, TEM is able to provide visible information on not only pore structures, but also defects. However, there are still some challenges in applying these useful techniques. For example, they put forward high requirements for the crystallinity of COFs, which are usually hard to meet. For TEM characterization, due to the organic nature of COFs, the samples are sensitive to the high energy electron beam which is usually required for high-resolution TEM. Nevertheless, these techniques provide guidance for the development of characterization methods for COFs with complicated structures. The structural elucidation of COFs *via* these techniques will be paid more and more attention.

Last but not least, the application development of heteropore COFs needs to be further strengthened. This includes two aspects. The first is to explore new applications exclusive to heteropore COFs by taking advantage of their unique hierarchical structures, as this will lead to new functions and applications of COFs. The pore structure heterogeneity of heteropore COFs lays a solid foundation for developing functional heterogeneity, which creates possibilities for fabrication of advanced materials, for example, composite materials to simultaneously take up/release different guests in/from different kinds of pores, even for those which are incompatible, and multifunctional materials through independently functionalizing different kinds of pores. On the other side, as porous materials, heteropore COFs can also be applied in many fields which have been explored for COFs with uniform pores. However, their hierarchical frameworks may be beneficial for their functions and thus make them superior over their single-pore congeners in applications such as catalysis, adsorption, separation, transportation, and so on. Such advantages certainly deserve to be extensively exploited. In this context, heteropore COFs with a large difference in pore size scales, for example, the coexistence of micropores and mesopores, should be more attractive.

In summary, after more than five years of development, heteropore COFs with various structures have been constructed. The unique properties and applications of heteropore COFs have also been discovered. Boosted by these achievements, this fascinating area will enter a new stage of development. In this context, we believe that more and more hierarchically porous COFs with new topologies, improved properties and various applications, especially applications exclusive to their structures, will be reported in the coming years.

Conflicts of interest

There are no conflicts to declare.

References

1 T. J. Barton, L. M. Bull, W. G. Klemperer, D. A. Loy, B. McEnaney, M. Misono, P. A. Monson, G. Pez, G. W. Scherer, J. C. Vartuli and O. M. Yaghi, *Chem. Mater.*, 1999, **11**, 2633–2656.
2 M. E. Davis, *Nature*, 2002, **417**, 813–821.
3 C. S. Diercks and O. M. Yaghi, *Science*, 2017, **355**, eaal1585.

4 S. Kandambeth, K. Dey and R. Banerjee, *J. Am. Chem. Soc.*, 2019, **141**, 1807–1822.

5 K. Geng, T. He, R. Liu, S. Dalapati, K. T. Tan, Z. Li, S. Tao, Y. Gong, Q. Jiang and D. Jiang, *Chem. Rev.*, 2020, **120**, DOI: 10.1021/acs.chemrev.9b00550.

6 Y. Xu, S. Jin, H. Xu, A. Nagai and D. Jiang, *Chem. Soc. Rev.*, 2013, **42**, 8012–8031.

7 A. I. Cooper, *Adv. Mater.*, 2009, **21**, 1291–1295.

8 L. Tan and B. Tan, *Chem. Soc. Rev.*, 2017, **46**, 3322–3356.

9 L. J. Abbott and C. M. Colina, *Macromolecules*, 2014, **47**, 5409–5415.

10 Y. Yuan and G. Zhu, *ACS Cent. Sci.*, 2019, **5**, 409–418.

11 N. B. McKeown and P. M. Budd, *Chem. Soc. Rev.*, 2006, **35**, 675–683.

12 D. Ramimoghadam, E. M. Gray and C. J. Webb, *Int. J. Hydrogen Energy*, 2016, **41**, 16944–16965.

13 J.-R. Song, J. Sun, J. Liu, Z.-T. Huang and Q.-Y. Zheng, *Chem. Commun.*, 2014, **50**, 788–791.

14 L. A. Baldwin, J. W. Crowe, D. A. Pyles and P. L. McGrier, *J. Am. Chem. Soc.*, 2016, **138**, 15134–15137.

15 Y. Zeng, R. Zou and Y. Zhao, *Adv. Mater.*, 2016, **28**, 2855–2873.

16 H. Furukawa and O. M. Yaghi, *J. Am. Chem. Soc.*, 2009, **131**, 8875–8883.

17 S. Ghosh and J. K. Singh, *Int. J. Hydrogen Energy*, 2019, **44**, 1782–1796.

18 Z. Kang, Y. Peng, Y. Qian, D. Yuan, M. A. Addicoat, T. Heine, Z. Hu, L. Tee, Z. Guo and D. Zhao, *Chem. Mater.*, 2016, **28**, 1277–1285.

19 H. Ma, H. Ren, S. Meng, Z. Yan, H. Zhao, F. Sun and G. Zhu, *Chem. Commun.*, 2013, **49**, 9773–9775.

20 S. Zhang, Y. Zheng, H. An, B. Aguila, C.-X. Yang, Y. Dong, W. Xie, P. Cheng, Z. Zhang, Y. Chen and S. Ma, *Angew. Chem., Int. Ed.*, 2018, **57**, 16754–16759.

21 C. Gao, J. Li, S. Yin, G. Lin, T. Ma, Y. Meng, J. Sun and C. Wang, *Angew. Chem., Int. Ed.*, 2019, **58**, 9770–9775.

22 J. Huang, X. Han, S. Yang, Y. Cao, C. Yuan, Y. Liu, J. Wang and Y. Cui, *J. Am. Chem. Soc.*, 2019, **141**, 8996–9003.

23 G. Lin, H. Ding, D. Yuan, B. Wang and C. Wang, *J. Am. Chem. Soc.*, 2016, **138**, 3302–3305.

24 S.-Y. Ding, M. Dong, Y.-W. Wang, Y.-T. Chen, H.-Z. Wang, C.-Y. Su and W. Wang, *J. Am. Chem. Soc.*, 2016, **138**, 3031–3037.

25 Q. Gao, X. Li, G.-H. Ning, K. Leng, B. Tian, C. Liu, W. Tang, H.-S. Xu and K. P. Loh, *Chem. Commun.*, 2018, **54**, 2349–2352.

26 P. Albacete, A. López-Moreno, S. Mena-Hernando, A. E. Platero-Prats, E. M. Pérez and F. Zamora, *Chem. Commun.*, 2019, **55**, 1382–1385.

27 P. Wang, M. Kang, S. Sun, Q. Liu, Z. Zhang and S. Fang, *Chin. J. Chem.*, 2014, **32**, 838–843.

28 Y. Peng, Y. Huang, Y. Zhu, B. Chen, L. Wang, Z. Lai, Z. Zhang, M. Zhao, C. Tan, N. Yang, F. Shao, Y. Han and H. Zhang, *J. Am. Chem. Soc.*, 2017, **139**, 8698–8704.

29 Q. Fang, S. Gu, J. Zheng, Z. Zhuang, S. Qiu and Y. Yan, *Angew. Chem., Int. Ed.*, 2014, **53**, 2878–2882.

30 P.-F. Wei, M.-Z. Qi, Z.-P. Wang, S.-Y. Ding, W. Yu, Q. Liu, L.-K. Wang, H.-Z. Wang, W.-K. An and W. Wang, *J. Am. Chem. Soc.*, 2018, **140**, 4623–4631.

31 S. Lin, C. S. Diercks, Y.-B. Zhang, N. Kornienko, E. M. Nichols, Y. Zhao, A. R. Paris, D. Kim, P. Yang, O. M. Yaghi and C. J. Chang, *Science*, 2015, **349**, 1208–1213.

32 X. Wang, X. Han, J. Zhang, X. Wu, Y. Liu and Y. Cui, *J. Am. Chem. Soc.*, 2016, **138**, 12332–12335.

33 G. Liu, J. Sheng and Y. Zhao, *Sci. China: Chem.*, 2017, **60**, 1015–1022.

34 S. Yan, X. Guan, H. Li, D. Li, M. Xue, Y. Yan, V. Valtchev, S. Qiu and Q. Fang, *J. Am. Chem. Soc.*, 2019, **141**, 2920–2924.

35 X. Zhao, P. Pachfule, S. Li, T. Langenhahn, M. Ye, C. Schlesiger, S. Praetz, J. Schmidt and A. Thomas, *J. Am. Chem. Soc.*, 2019, **141**, 6623–6630.

36 S. Lu, Y. Hu, S. Wan, R. McCaffrey, Y. Jin, H. Gu and W. Zhang, *J. Am. Chem. Soc.*, 2017, **139**, 17082–17088.

37 S. Chandra, T. Kundu, S. Kandambeth, R. BabaRao, Y. Marathe, S. M. Kunjir and R. Banerjee, *J. Am. Chem. Soc.*, 2014, **136**, 6570–6573.

38 H. Xu, S. Tao and D. Jiang, *Nat. Mater.*, 2016, **15**, 722–726.

39 Q. Fang, J. Wang, S. Gu, R. B. Kaspar, Z. Zhuang, J. Zheng, H. Guo, S. Qiu and Y. Yan, *J. Am. Chem. Soc.*, 2015, **137**, 8352–8355.

40 V. S. Vyas, M. Vishwakarma, I. Moudrakovski, F. Haase, G. Savasci, C. Ochsenfeld, J. P. Spatz and B. V. Lotsch, *Adv. Mater.*, 2016, **28**, 8749–8754.

41 G. Zhang, X. Li, Q. Liao, Y. Liu, K. Xi, W. Huang and X. Jia, *Nat. Commun.*, 2018, **9**, 2785.

42 S. Mitra, H. S. Sasmal, T. Kundu, S. Kandambeth, K. Illath, D. D. Díaz and R. Banerjee, *J. Am. Chem. Soc.*, 2017, **139**, 4513–4520.

43 C. R. DeBlase, K. E. Silberstein, T.-T. Truong, H. D. Abruña and W. R. Dichtel, *J. Am. Chem. Soc.*, 2013, **135**, 16821–16824.

44 H. Liao, H. Wang, H. Ding, X. Meng, H. Xu, B. Wang, X. Ai and C. Wang, *J. Mater. Chem. A*, 2016, **4**, 7416–7421.

45 F. Xu, H. Xu, X. Chen, D. Wu, Y. Wu, H. Liu, C. Gu, R. Fu and D. Jiang, *Angew. Chem., Int. Ed.*, 2015, **54**, 6814–6818.

46 C. R. DeBlase, K. Hernández-Burgos, K. E. Silberstein, G. G. Rodríguez-Calero, R. P. Bisbey, H. D. Abruña and W. R. Dichtel, *ACS Nano*, 2015, **9**, 3178–3183.

47 S. Wang, Q. Wang, P. Shao, Y. Han, X. Gao, L. Ma, S. Yuan, X. Ma, J. Zhou, X. Feng and B. Wang, *J. Am. Chem. Soc.*, 2017, **139**, 4258–4261.

48 C. R. Mulzer, L. Shen, R. P. Bisbey, J. R. McKone, N. Zhang, H. D. Abruña and W. R. Dichtel, *ACS Cent. Sci.*, 2016, **2**, 667–673.

49 Y. Hu, N. Dunlap, S. Wan, S. Lu, S. Huang, I. Sellinger, M. Ortiz, Y. Jin, S. Lee and W. Zhang, *J. Am. Chem. Soc.*, 2019, **141**, 7518–7525.

50 Y. Zhang, J. Duan, D. Ma, P. Li, S. Li, H. Li, J. Zhou, X. Ma, X. Feng and B. Wang, *Angew. Chem., Int. Ed.*, 2017, **56**, 16313–16317.

51 L. Chen, K. Furukawa, J. Gao, A. Nagai, T. Nakamura, Y. Dong and D. Jiang, *J. Am. Chem. Soc.*, 2014, **136**, 9806–9809.

3948 | *Chem. Soc. Rev.*, 2020, **49**, 3920–3951

This journal is © The Royal Society of Chemistry 2020

52 L. Yang and D.-C. Wei, *Chin. Chem. Lett.*, 2016, **27**, 1395–1404.

53 M. Calik, F. Auras, L. M. Salonen, K. Bader, I. Grill, M. Handloser, D. D. Medina, M. Dogru, F. Löbermann, D. Trauner, A. Hartschuh and T. Bein, *J. Am. Chem. Soc.*, 2014, **136**, 17802–17807.

54 X. Wang, L. Chen, S. Y. Chong, M. A. Little, Y. Wu, W.-H. Zhu, R. Clowes, Y. Yan, M. A. Zwijnenburg, R. S. Sprick and A. I. Cooper, *Nat. Chem.*, 2018, **10**, 1180–1189.

55 J. I. Feldblyum, C. H. McCreery, S. C. Andrews, T. Kurosawa, E. J. G. Santos, V. Duong, L. Fang, A. L. Ayzner and Z. Bao, *Chem. Commun.*, 2015, **51**, 13894–13897.

56 L. Ma, S. Wang, X. Feng and B. Wang, *Chin. Chem. Lett.*, 2016, **27**, 1383–1394.

57 Y. Yusran, X. Guan, H. Li, Q. Fang and S. Qiu, *Natl. Sci. Rev.*, 2020, **7**, 170–190.

58 A. P. Côté, A. I. Benin, N. W. Ockwig, M. O'Keeffe, A. J. Matzger and O. M. Yaghi, *Science*, 2005, **310**, 1166–1170.

59 S. Wan, J. Guo, J. Kim, H. Ihee and D. Jiang, *Angew. Chem., Int. Ed.*, 2008, **47**, 8826–8830.

60 L. M. Lanni, R. W. Tilford, M. Bharathy and J. J. Lavigne, *J. Am. Chem. Soc.*, 2011, **133**, 13975–13983.

61 E. L. Spitler, B. T. Koo, J. L. Novotney, J. W. Colson, F. J. Uribe-Romo, G. D. Gutierrez, P. Clancy and W. R. Dichtel, *J. Am. Chem. Soc.*, 2011, **133**, 19416–19421.

62 L. Stegbauer, K. Schwinghammer and B. V. Lotsch, *Chem. Sci.*, 2014, **5**, 2789–2793.

63 M. Matsumoto, R. R. Dasari, W. Ji, C. H. Feriante, T. C. Parker, S. R. Marder and W. R. Dichtel, *J. Am. Chem. Soc.*, 2017, **139**, 4999–5002.

64 L. Bai, S. Z. F. Phua, W. Q. Lim, A. Jana, Z. Luo, H. P. Tham, L. Zhao, Q. Gao and Y. Zhao, *Chem. Commun.*, 2016, **52**, 4128–4131.

65 S. Wei, F. Zhang, W. Zhang, P. Qiang, K. Yu, X. Fu, D. Wu, S. Bi and F. Zhang, *J. Am. Chem. Soc.*, 2019, **141**, 14272–14279.

66 L. Bai, Q. Gao and Y. Zhao, *J. Mater. Chem. A*, 2016, **4**, 14106–14110.

67 S. Jin, X. Ding, X. Feng, M. Supur, K. Furukawa, S. Takahashi, M. Addicoat, M. E. El-Khouly, T. Nakamura, S. Irle, S. Fukuzumi, A. Nagai and D. Jiang, *Angew. Chem., Int. Ed.*, 2013, **52**, 2017–2021.

68 E. L. Spitler, J. W. Colson, F. J. Uribe-Romo, A. R. Woll, M. R. Giovino, A. Saldivar and W. R. Dichtel, *Angew. Chem., Int. Ed.*, 2012, **51**, 2623–2627.

69 B. Gole, V. Stepanenko, S. Rager, M. Grüne, D. D. Medina, T. Bein, F. Würthner and F. Beuerle, *Angew. Chem., Int. Ed.*, 2018, **57**, 846–850.

70 V. S. P. K. Neti, X. Wu, S. Deng and L. Echegoyen, *Polym. Chem.*, 2013, **4**, 4566–4569.

71 S. Wan, F. Gándara, A. Asano, H. Furukawa, A. Saeki, S. K. Dey, L. Liao, M. W. Ambrogio, Y. Y. Botros, X. Duan, S. Seki, J. F. Stoddart and O. M. Yaghi, *Chem. Mater.*, 2011, **23**, 4094–4097.

72 T. Joshi, C. Chen, H. Li, C. S. Diercks, G. Wang, P. J. Waller, H. Li, J.-L. Bredas, O. M. Yaghi and M. F. Crommie, *Adv. Mater.*, 2019, **31**, 1805941.

73 H. Ding, Y. Li, H. Hu, Y. Sun, J. Wang, C. Wang, C. Wang, G. Zhang, B. Wang, W. Xu and D. Zhang, *Chem. – Eur. J.*, 2014, **20**, 14614–14618.

74 S.-L. Cai, Y.-B. Zhang, A. B. Pun, B. He, J. Yang, F. M. Toma, I. D. Sharp, O. M. Yaghi, J. Fan, S.-R. Zheng, W.-G. Zhang and Y. Liu, *Chem. Sci.*, 2014, **5**, 4693–4700.

75 E. Jin, M. Asada, Q. Xu, S. Dalapati, M. A. Addicoat, M. A. Brady, H. Xu, T. Nakamura, T. Heine, Q. Chen and D. Jiang, *Science*, 2017, **357**, 673–676.

76 B. Dong, L. Wang, S. Zhao, R. Ge, X. Song, Y. Wang and Y. Gao, *Chem. Commun.*, 2016, **52**, 7082–7085.

77 S. B. Alahakoon, C. M. Thompson, A. X. Nguyen, G. Occhialini, G. T. McCandless and R. A. Smaldone, *Chem. Commun.*, 2016, **52**, 2843–2845.

78 S. Dalapati, M. Addicoat, S. Jin, T. Sakurai, J. Gao, H. Xu, S. Irle, S. Seki and D. Jiang, *Nat. Commun.*, 2015, **6**, 7786.

79 S.-L. Cai, K. Zhang, J.-B. Tan, S. Wang, S.-R. Zheng, J. Fan, Y. Yu, W.-G. Zhang and Y. Liu, *ACS Macro Lett.*, 2016, **5**, 1348–1352.

80 S.-Y. Ding and W. Wang, *Chem. Soc. Rev.*, 2013, **42**, 548–568.

81 Y. Song, Q. Sun, B. Aguila and S. Ma, *Adv. Sci.*, 2019, **6**, 1801410.

82 M. S. Lohse and T. Bein, *Adv. Funct. Mater.*, 2018, **28**, 1705553.

83 N. Huang, P. Wang and D. Jiang, *Nat. Rev. Mater.*, 2016, **1**, 16068.

84 X.-Y. Yang, L.-H. Chen, Y. Li, J. C. Rooke, C. Sanchez and B.-L. Su, *Chem. Soc. Rev.*, 2017, **46**, 481–558.

85 S. Lopez-Orozco, A. Inayat, A. Schwab, T. Selvam and W. Schwieger, *Adv. Mater.*, 2011, **23**, 2602–2615.

86 N. D. Petkovich and A. Stein, *Chem. Soc. Rev.*, 2013, **42**, 3721–3739.

87 Y. Li, Z.-Y. Fu and B.-L. Su, *Adv. Funct. Mater.*, 2012, **22**, 4634–4667.

88 T.-Y. Zhou, S.-Q. Xu, Q. Wen, Z.-F. Pang and X. Zhao, *J. Am. Chem. Soc.*, 2014, **136**, 15885–15888.

89 Y. Jin, Y. Hu and W. Zhang, *Nat. Rev. Chem.*, 2017, **1**, 0056.

90 R.-R. Liang and X. Zhao, *Org. Chem. Front.*, 2018, **5**, 3341–3356.

91 G. Zhang, M. Tsujimoto, D. Packwood, N. T. Duong, Y. Nishiyama, K. Kadota, S. Kitagawa and S. Horike, *J. Am. Chem. Soc.*, 2018, **140**, 2602–2609.

92 S. Karak, K. Dey, A. Torris, A. Halder, S. Bera, F. Kanheerampockil and R. Banerjee, *J. Am. Chem. Soc.*, 2019, **141**, 7572–7581.

93 L. Ascherl, T. Sick, J. T. Margraf, S. H. Lapidus, M. Calik, C. Hettstedt, K. Karaghiosoff, M. Döblinger, T. Clark, K. W. Chapman, F. Auras and T. Bein, *Nat. Chem.*, 2016, **8**, 310–316.

94 P. Wang, Q. Xu, Z. Li, W. Jiang, Q. Jiang and D. Jiang, *Adv. Mater.*, 2018, **30**, 1801991.

95 M. Zhang, L. Li, Q. Lin, M. Tang, Y. Wu and C. Ke, *J. Am. Chem. Soc.*, 2019, **141**, 5154–5158.

96 Z.-F. Pang, S.-Q. Xu, T.-Y. Zhou, R.-R. Liang, T.-G. Zhan and X. Zhao, *J. Am. Chem. Soc.*, 2016, **138**, 4710–4713.

This journal is © The Royal Society of Chemistry 2020

Chem. Soc. Rev., 2020, **49**, 3920–3951 | **3949**

97 Q. Chen, J. Tang and Q. Fang, *Chem. J. Chin. Univ.*, 2018, **39**, 2357–2362.

98 T. Sick, A. G. Hufnagel, J. Kampmann, I. Kondofersky, M. Calik, J. M. Rotter, A. Evans, M. Döblinger, S. Herbert, K. Peters, D. Böhm, P. Knochel, D. D. Medina, D. Fattakhova-Rohlfing and T. Bein, *J. Am. Chem. Soc.*, 2018, **140**, 2085–2092.

99 J. M. Rotter, S. Weinberger, J. Kampmann, T. Sick, M. Shalom, T. Bein and D. D. Medina, *Chem. Mater.*, 2019, **31**, 10008–10016.

100 A. C. Jakowetz, T. F. Hinrichsen, L. Ascherl, T. Sick, M. Calik, F. Auras, D. D. Medina, R. H. Friend, A. Rao and T. Bein, *J. Am. Chem. Soc.*, 2019, **141**, 11565–11571.

101 N. Liu, L. Shi, X. Han, Q.-Y. Qi, Z.-Q. Wu and X. Zhao, *Chin. Chem. Lett.*, 2020, **31**, 386–390.

102 L. Guo, S. Jia, C. S. Diercks, X. Yang, S. A. Alshmimri and O. M. Yaghi, *Angew. Chem., Int. Ed.*, 2020, **59**, 2023–2027.

103 J. Dong, X. Li, S. B. Peh, Y. D. Yuan, Y. Wang, D. Ji, S. Peng, G. Liu, S. Ying, D. Yuan, J. Jiang, S. Ramakrishna and D. Zhao, *Chem. Mater.*, 2019, **31**, 146–160.

104 Z. Xie, B. Wang, Z. Yang, X. Yang, X. Yu, G. Xing, Y. Zhang and L. Chen, *Angew. Chem., Int. Ed.*, 2019, **58**, 15742–15746.

105 Y. Tian, S.-Q. Xu, C. Qian, Z.-F. Pang, G.-F. Jiang and X. Zhao, *Chem. Commun.*, 2016, **52**, 11704–11707.

106 Y. Tian, S.-Q. Xu, R.-R. Liang, C. Qian, G.-F. Jiang and X. Zhao, *CrystEngComm*, 2017, **19**, 4877–4881.

107 F.-Z. Cui, R.-R. Liang, Q.-Y. Qi, G.-F. Jiang and X. Zhao, *Adv. Sustainable Syst.*, 2019, **3**, 1800150.

108 L. Ascherl, E. W. Evans, J. Gorman, S. Orsborne, D. Bessinger, T. Bein, R. H. Friend and F. Auras, *J. Am. Chem. Soc.*, 2019, **141**, 15693–15699.

109 F.-Z. Cui, J.-J. Xie, S.-Y. Jiang, S.-X. Gan, D.-L. Ma, R.-R. Liang, G.-F. Jiang and X. Zhao, *Chem. Commun.*, 2019, **55**, 4550–4553.

110 G. Das, B. P. Biswal, S. Kandambeth, V. Venkatesh, G. Kaur, M. Addicoat, T. Heine, S. Verma and R. Banerjee, *Chem. Sci.*, 2015, **6**, 3931–3939.

111 S. Dalapati, S. Jin, J. Gao, Y. Xu, A. Nagai and D. Jiang, *J. Am. Chem. Soc.*, 2013, **135**, 17310–17313.

112 M. G. Rabbani, A. K. Sekizkardes, Z. Kahveci, T. E. Reich, R. Ding and H. M. El-Kaderi, *Chem. – Eur. J.*, 2013, **19**, 3324–3328.

113 Z.-F. Pang, T.-Y. Zhou, R.-R. Liang, Q.-Y. Qi and X. Zhao, *Chem. Sci.*, 2017, **8**, 3866–3870.

114 Y.-P. Mo, X.-H. Liu and D. Wang, *ACS Nano*, 2017, **11**, 11694–11700.

115 R.-R. Liang, F.-Z. Cui, R.-H. A, Q.-Y. Qi and X. Zhao, *CCS Chem.*, 2020, **2**, 139–145.

116 S. Dalapati, E. Jin, M. Addicoat, T. Heine and D. Jiang, *J. Am. Chem. Soc.*, 2016, **138**, 5797–5800.

117 P. J. Waller, S. J. Lyle, T. M. O. Popp, C. S. Diercks, J. A. Reimer and O. M. Yaghi, *J. Am. Chem. Soc.*, 2016, **138**, 15519–15522.

118 S. J. Lyle, T. M. O. Popp, P. J. Waller, X. Pei, J. A. Reimer and O. M. Yaghi, *J. Am. Chem. Soc.*, 2019, **141**, 11253–11258.

119 S.-Y. Jiang, S.-X. Gan, X. Zhang, H. Li, Q.-Y. Qi, F.-Z. Cui, J. Lu and X. Zhao, *J. Am. Chem. Soc.*, 2019, **141**, 14981–14986.

120 M. Lu, J. Liu, Q. Li, M. Zhang, M. Liu, J.-L. Wang, D.-Q. Yuan and Y.-Q. Lan, *Angew. Chem., Int. Ed.*, 2019, **58**, 12392–12397.

121 T. Banerjee, F. Haase, S. Trenker, B. P. Biswal, G. Savasci, V. Duppel, I. Moudrakovski, C. Ochsenfeld and B. V. Lotsch, *Nat. Commun.*, 2019, **10**, 2689.

122 B. Zhang, H. Mao, R. Matheu, J. A. Reimer, S. A. Alshmimri, S. Alshihri and O. M. Yaghi, *J. Am. Chem. Soc.*, 2019, **141**, 11420–11424.

123 Q. Gao, X. Li, G.-H. Ning, H.-S. Xu, C. Liu, B. Tian, W. Tang and K. P. Loh, *Chem. Mater.*, 2018, **30**, 1762–1768.

124 Y. Zhu, S. Wan, Y. Jin and W. Zhang, *J. Am. Chem. Soc.*, 2015, **137**, 13772–13775.

125 M.-W. Zhu, S.-Q. Xu, X.-Z. Wang, Y. Chen, L. Dai and X. Zhao, *Chem. Commun.*, 2018, **54**, 2308–2311.

126 S. K. Yang, A. V. Ambade and M. Weck, *J. Am. Chem. Soc.*, 2010, **132**, 1637–1645.

127 J.-F. Ayme, J. E. Beves, D. A. Leigh, R. T. McBurney, K. Rissanen and D. Schultz, *Nat. Chem.*, 2012, **4**, 15–20.

128 K.-D. Zhang and S. Matile, *Angew. Chem., Int. Ed.*, 2015, **54**, 8980–8983.

129 A. Wilson, G. Gasparini and S. Matile, *Chem. Soc. Rev.*, 2014, **43**, 1948–1962.

130 W. Wang, Y. Zhang, B. Sun, L.-J. Chen, X.-D. Xu, M. Wang, X. Li, Y. Yu, W. Jiang and H.-B. Yang, *Chem. Sci.*, 2014, **5**, 4554–4560.

131 N. Luisier, K. Schenk and K. Severin, *Chem. Commun.*, 2014, **50**, 10233–10236.

132 K. D. Okochi, G. S. Han, I. M. Aldridge, Y. Liu and W. Zhang, *Org. Lett.*, 2013, **15**, 4296–4299.

133 Z. He, W. Jiang and C. A. Schalley, *Chem. Soc. Rev.*, 2015, **44**, 779–789.

134 Y. Zeng, R. Zou, Z. Luo, H. Zhang, X. Yao, X. Ma, R. Zou and Y. Zhao, *J. Am. Chem. Soc.*, 2015, **137**, 1020–1023.

135 X. Chen, M. Addicoat, E. Jin, H. Xu, T. Hayashi, F. Xu, N. Huang, S. Irle and D. Jiang, *Sci. Rep.*, 2015, **5**, 14650.

136 H. L. Nguyen, F. Gándara, H. Furukawa, T. L. H. Doan, K. E. Cordova and O. M. Yaghi, *J. Am. Chem. Soc.*, 2016, **138**, 4330–4333.

137 H. Li, Q.-Y. Qi, X. Zhao, G. Li, X. Chen, H.-J. Zhang and J. Lin, *Polym. Chem.*, 2018, **9**, 4288–4293.

138 R.-R. Liang, S.-Q. Xu, Z.-F. Pang, Q.-Y. Qi and X. Zhao, *Chem. Commun.*, 2018, **54**, 880–883.

139 D. N. Bunck and W. R. Dichtel, *Chem. – Eur. J.*, 2013, **19**, 818–827.

140 C. Qian, S.-Q. Xu, G.-F. Jiang, T.-G. Zhan and X. Zhao, *Chem. – Eur. J.*, 2016, **22**, 17784–17789.

141 C. Qian, Q.-Y. Qi, G.-F. Jiang, F.-Z. Cui, Y. Tian and X. Zhao, *J. Am. Chem. Soc.*, 2017, **139**, 6736–6743.

142 P. J. Waller, Y. S. AlFaraj, C. S. Diercks, N. N. Jarenwattananon and O. M. Yaghi, *J. Am. Chem. Soc.*, 2018, **140**, 9099–9103.

143 M. C. Daugherty, E. Vitaku, R. L. Li, A. M. Evans, A. D. Chavez and W. R. Dichtel, *Chem. Commun.*, 2019, **55**, 2680–2683.

144 H.-L. Qian, Y. Li and X.-P. Yan, *J. Mater. Chem. A*, 2018, **6**, 17307–17311.

145 Z. Li, X. Ding, Y. Feng, W. Feng and B.-H. Han, *Macromolecules*, 2019, **52**, 1257–1265.

146 S.-L. Cai, Z.-H. He, X.-L. Li, K. Zhang, S.-R. Zheng, J. Fan, Y. Liu and W.-G. Zhang, *Chem. Commun.*, 2019, **55**, 13454–13457.

147 R.-R. Liang, S.-Q. Xu, L. Zhang, R.-H. A, P. Chen, F.-Z. Cui, Q.-Y. Qi, J. Sun and X. Zhao, *Nat. Commun.*, 2019, **10**, 4609.

148 C. Qian, E.-C. Liu, Q.-Y. Qi, K. Xu, G.-F. Jiang and X. Zhao, *Polym. Chem.*, 2018, **9**, 279–283.

149 S.-Q. Xu, T.-G. Zhan, Q. Wen, Z.-F. Pang and X. Zhao, *ACS Macro Lett.*, 2016, **5**, 99–102.

150 P. Wang, X. Chen, Q. Jiang, M. Addicoat, N. Huang, S. Dalapati, T. Heine, F. Huo and D. Jiang, *Angew. Chem., Int. Ed.*, 2019, **58**, 15922–15927.

151 S. Xu, G. Wang, B. P. Biswal, M. Addicoat, S. Paasch, W. Sheng, X. Zhuang, E. Brunner, T. Heine, R. Berger and X. Feng, *Angew. Chem., Int. Ed.*, 2019, **58**, 849–853.

152 K. Wang, L.-M. Yang, X. Wang, L. Guo, G. Cheng, C. Zhang, S. Jin, B. Tan and A. Cooper, *Angew. Chem., Int. Ed.*, 2017, **56**, 14149–14153.

153 P. Kuhn, M. Antonietti and A. Thomas, *Angew. Chem., Int. Ed.*, 2008, **47**, 3450–3453.

154 Z.-J. Yin, S.-Q. Xu, T.-G. Zhan, Q.-Y. Qi, Z.-Q. Wu and X. Zhao, *Chem. Commun.*, 2017, **53**, 7266–7269.

155 Y. Li, Q. Chen, T. Xu, Z. Xie, J. Liu, X. Yu, S. Ma, T. Qin and L. Chen, *J. Am. Chem. Soc.*, 2019, **141**, 13822–13828.

156 X. Feng, Y. Dong and D. Jiang, *CrystEngComm*, 2013, **15**, 1508–1511.

157 H. Yang, Y. Du, S. Wan, G. D. Trahan, Y. Jin and W. Zhang, *Chem. Sci.*, 2015, **6**, 4049–4053.

158 L. A. Baldwin, J. W. Crowe, M. D. Shannon, C. P. Jaroniec and P. L. McGrier, *Chem. Mater.*, 2015, **27**, 6169–6172.

159 Y. Du, H. Yang, J. M. Whiteley, S. Wan, Y. Jin, S.-H. Lee and W. Zhang, *Angew. Chem., Int. Ed.*, 2016, **55**, 1737–1741.

160 J. W. Crowe, L. A. Baldwin and P. L. McGrier, *J. Am. Chem. Soc.*, 2016, **138**, 10120–10123.

161 Q. Sun, B. Aguila, P. C. Lan and S. Ma, *Adv. Mater.*, 2019, **31**, 1900008.

162 Q. Sun, C.-W. Fu, B. Aguila, J. Perman, S. Wang, H.-Y. Huang, F.-S. Xiao and S. Ma, *J. Am. Chem. Soc.*, 2018, **140**, 984–992.

163 R.-R. Liang, R.-H. A, S.-Q. Xu, Q.-Y. Qi and X. Zhao, *J. Am. Chem. Soc.*, 2020, **142**, 70–74.

164 W. Wang, *Chin. J. Org. Chem.*, 2020, **40**, 545–546.

165 A. M. Evans, L. R. Parent, N. C. Flanders, R. P. Bisbey, E. Vitaku, M. S. Kirschner, R. D. Schaller, L. X. Chen, N. C. Gianneschi and W. R. Dichtel, *Science*, 2018, **361**, 52–57.

166 T. Ma, E. A. Kapustin, S. X. Yin, L. Liang, Z. Zhou, J. Niu, L.-H. Li, Y. Wang, J. Su, J. Li, X. Wang, W. D. Wang, W. Wang, J. Sun and O. M. Yaghi, *Science*, 2018, **361**, 48–52.

This journal is © The Royal Society of Chemistry 2020

Chem. Soc. Rev., 2020, **49**, 3920–3951 | **3951**